Effect of IGFBP7 on Cardiac/Renal Vascular Remodeling in Diabetes Mellitus

Yiqing Huang, BSc

A Thesis submitted to the University of Ottawa
in partial Fulfilment of the requirements for the Master of Science Degree in Cellular Molecular Medicine

Department of Cellular and Molecular Medicine

Faculty of Medicine

University of Ottawa

Abstract

Insulin-like growth factor (IGF) Binding Protein 7 (IGFBP7) is a regulatory protein of IGF-1 signalling, and has also been demonstrated to be excellent cardiac and acute renal injury biomarkers. But the biological effect of IGFBP7 in diabetic kidney disease (DKD) is still elusive. Utilizing a pre-established DKD mouse model, we found that Igfbp7 was significantly elevated in both serum and kidney tissues of affected mice. In kidney, Igfbp7 was enriched in pericytes and podocytes but not endothelial cells in the glomerulus, suggesting the potential involvement of IGFBP7 in maintaining microvascular networks and glomerular filtration barrier. Our study indicates that IGFBP7 can be applied as a DKD biomarker, as well as its important role in the glomerulus, which provides novel insights about how IGFBP7 could participate in the progression of DKD.

Acknowledgements

I would like to thank Dr. Peter Liu, Dr. Liyong Zhang and Qiujiang Du for providing me with the training, materials, and equipment to carry out experiments for this project. I would also like to thank Dr. Natasha Trzaskalski and Dr. Edwige Martin-Valiente for additional support and guidance throughout my training experience. Extended thank you to all of the trainee fellows for the accompany of this exciting journey.

I would like to thank my Thesis Advisory Committee members, Dr. Han Kim and Dr. Kevin Burns for providing guidance and support throughout my master's degree.

I would like to thank the research fellows in the Kidney Research Center——Dr. Dylan Burger and Chloé Landry for providing the mouse strain; Chet Holterman for providing materials and equipment; Dr. Chris Kenney and Dr. Alexey Gutsol for guidance in the knowledge of nephrology. Your knowledge and expertise have been valuable for me to explore a brand-new area.

I would like to thank Xiaoling Zhao from the High Resolution Cell Imaging Core Facility. Thanks for the guidance and support in histology. Your expertise and kindness made my MSc so enjoyable.

Above all, I would like to express my most heartfelt thanks to my parents for generous financial support, which allowed me to start a new life in Canada. I would not have accomplished this milestone without you.

Funding

This work was supported by the Canada First Research Excellence Fund for the Brain-Heart Interconnectome; Government of Canada through Genome Canada and Ontario Genomics; and Brain Canada Foundation, and Heart and Stroke Foundation of Canada for Heart-Brain Connection IMPACT Award to Dr. Peter Liu. Yiqing Huang was a recipient of a Brain-Heart Interconnectome (BHI) scholarship.

Table of Contents

List of Abbreviations

ACEI	Angiotensin-converting Enzyme Inhibitor
AKI	Acute Kidney Injury
ARB	Angiotensin II Receptor Blocker
AUC	Area Under the Curve
BP	Blood Pressure
CAD	Coronary Artery Disease
CKD	Chronic Kidney Disease
CVD	Cardiovascular Disease
DKD	Diabetic Kidney Disease
eGFR	estimated Glomerular Filtration Rate
ELISA	Enzyme-linked Immunosorbent Assay
ESKD	End-stage Kidney Disease
GEC	Glomerular Endothelial Cell
HDL	High-density Lipoprotein
HF	Heart Failure
HFpEF	Heart Failure with Preserved Ejection Fraction
HFrEF	Heart Failure with Reduced Ejection Fraction
hsTnI	Highly Sensitive Troponin I
Htra3	High-temperature Requirement A Serine Peptidase 3
HW	Heart Weight
IGF	Insulin-like Growth Factor
IGFBP7	Insulin-like Growth Factor Binding Protein 7
IVRT	Isovolumic Relaxation Time
KW	Kidney Weight
LAVi	Left Atrial Volume index
LDL	Low-density Lipoprotein

LVPW;s	End-systolic Left Ventricular Posterior Wall Thickness
LVPW;d	End-diastolic Left Ventricular Posterior Wall Thickness
LW	Lung Weight
MC	Mesangial Cell
MI	Myocardial Infarction
OHCA	Out-of-hospital Cardiac Arrest
PAS	Periodic-acid Schiff
PBS	Phosphate Buffered Saline
PEC	Parietal Epithelial Cell
PIIINP	Pro-collagen Type III Amino-terminal Peptide
PKM2	Pyruvate Kinase M2
RAAS	Renin–Angiotensin–Aldosterone System
RRT	Renal Replacement Therapy
RVSP	Right Ventricular Systolic Pressure
STZ	Streptozotocin
TGF-β	Transforming Growth Factor-β
TIMP-2	Tissue Inhibitor of Metalloproteinases-2
TL	Tibia Length
TTRhRen	Transthyretin Human Renin
VO_{2max}	Peak Oxygen Consumption
WT	Wild-type

List of Tables

List of Figures

1. Introduction

1.1 The Function and Structure of the Kidney

Kidney is a bean-shaped organ that plays several important functions in the human body, including excretion of waste products, the control of blood pressure via the renin-angiotensin-aldosterone system, and reabsorption of critical molecules[1]. A mammal's kidney is highly vascularized and is estimated to filter around 20% of total cardiac output[2,3]. Blood filtration by the kidneys can generate, on average, 1 liter of urine per day in humans, which can be further concentrated along the nephrons[4].

The kidney is comprised of two regions: the cortex and medulla (**Figure 1A**). The cortex consists of renal corpuscles, convoluted tubules, straight tubules, collecting tubules, collecting ducts, and vasculature[1]. The medulla refers to the central and inner parts of the kidneys, which contain nephron loops, collecting ducts, vasa recta, and interstitium[5]. Nephrons, the functional units of the kidney, can vary from 1 million to 2.5 million per adult kidney[6]. A nephron is divided into a filtration unit called the renal corpuscle and a segmented reabsorption compartment called tubule[4]. Each renal corpuscle is comprised of a glomerulus and a double-layered epithelium called Bowman's capsule[1] (**Figure 1B**).

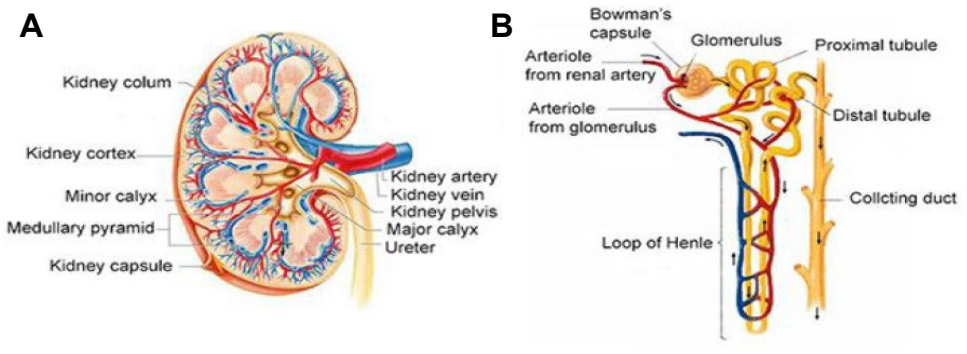

Figure 1 Illustration of kidney (A) and nephron (B) anatomical structures. Image credit: Saurus, H. P. Regulation of podocyte apoptosis in diabetic kidney disease–Role of SHIP2, PDK1 and CDK2. (2016).[7]

1.2 The Heterogeneity of Glomerular Cells

The glomerulus is mainly composed of four different cell types: the glomerular endothelial cells (GECs), podocytes, mesangial cells (MCs), and parietal epithelial cells (PECs). Podocytes are specialized perivascular cells that wrap around the exterior of glomerular capillaries[4]. GECs are widely studied for their function as regulating blood flow, coagulation, inflammation and vascular permeability[8]. MCs are perceived as glomerular pericytes and provide the structural support for the glomerular vasculature[4,9]. PECs cover the inner part of Bowman's capsule[4] (**Figure 2**).

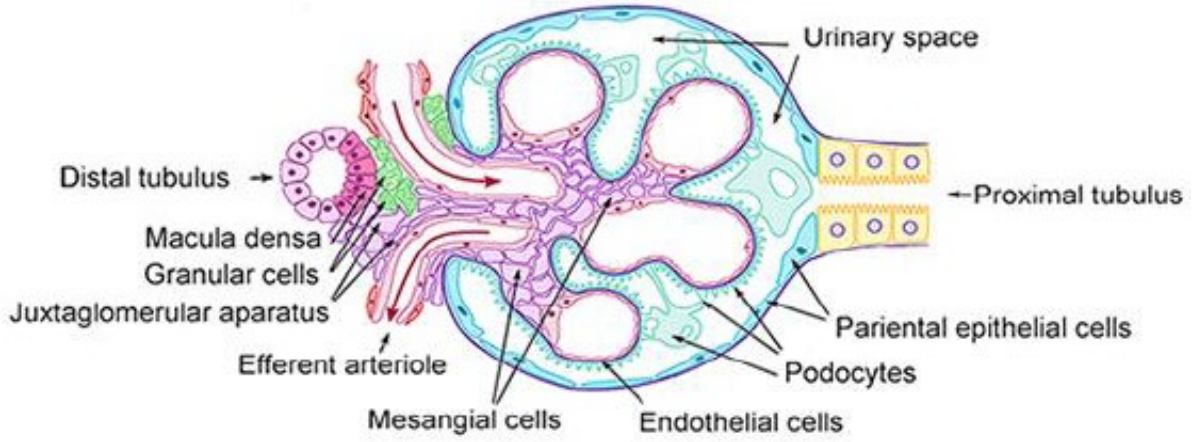

Figure 2 Different types of cells in the glomerulus. Image credit: Saurus, H. P. Regulation of podocyte apoptosis in diabetic kidney disease–Role of SHIP2, PDK1 and CDK2. (2016).[7]

1.3 Diabetic Kidney Disease (DKD)

Diabetes mellitus is characterized as a metabolic disorder with chronically high blood glucose levels (hyperglycemia) due to insulin insufficiency or lack of response to insulin[10]. With the prevalence of diabetes steadily rising every year, it is estimated to affect 12.2% of the adult population worldwide by the year 2045[11]. In Canada, it represents a significant public health burden as 3.4 million Canadians were living with diabetes in 2017-2018[12], or 9.6% of the population.

Diabetic kidney disease (DKD) is a prevalent microvascular complication that affects approximately 40% of individuals with diabetes[13]. It accounts for one-third of chronic kidney disease (CKD) cases[14,15]. In the context of end-stage kidney disease (ESKD), the final stage of CKD, DKD is considered as the primary etiology, contributing to 30-50% of ESKD cases globally[16].

First described by Mogensen in the 1980s, one of the early signs of DKD is the leakage of a small amount of albumin into the urine (30-300 mg per day), known as microalbuminuria. Macroalbuminuria is observed in advanced DKD as a larger amount of albumin becomes detectable in the urine (>300 mg per day), accompanied by a persistent decline in kidney function and renal impairment[17].

1.3.1 Histopathology of DKD

Glomerular changes reflect the effect of chronic hyperglycemia on renal function in DKD. At the early stage of DKD, glomerular hyperfiltration comes with glomerular hypertrophy, with glomerular volume enlarged 70% compared to the non-diabetic subjects[18]. Another characteristic change is the thickening of the glomerular basement membrane, which is caused by the interference of normal collagen turnover and the

deposition of extracellular matrix proteins. Relentless accumulation of matrix proteins results in mesangial expansion, which further damages the glomerular capillary loops[19]. Glomerulosclerosis can be observed at later stages as the glomeruli become solidified[20].

Apart from glomerular dysfunction, tubulointerstitial changes, such as tubular injury, interstitial fibrosis and tubular dilation, are often observed in DKD as key features of renal dysfunction. It is suggested that hyperglycemia and the accumulation of advanced glycation end-products may contribute to cellular stress, mitochondrial dysfunction, and activation of pro-apoptotic pathways, ultimately leading to tubular atrophy and apoptosis. Chronic hyperglycemia and other metabolic disturbances associated with diabetes also lead to the expansion of the tubular lumen (tubular dilation), in an attempt to facilitate tubular reabsorption in the presence of glomerular damage[19]. Tubulointerstitial fibrosis is widely considered the final contributor to renal dysfunction. Progressive renal scarring can be attributed to fibrogenic cells derived from various sources, including transformation of resident fibroblasts and mesenchymal stem cells, recruitment of fibroblasts from the bone marrow, and tubuloepithelial to mesenchymal trans-differentiation[21].

1.3.2 Risk Factors and Management of CKD

1.3.2.1 Hypertension and Blood Pressure Control

Elevated blood pressure increases the risk for CKD in both type 1 and type 2 diabetes[22–24]. The impact of hypertension on the loss of renal function can be partially explained by the loss of renal autoregulation in diabetes, thus exposing vulnerable glomerular capillaries to systemic pressure[25,26]. With the correlation between blood pressure and the onset of renal failure, lowering blood pressure is widely acknowledged as the most effective treatment for CKD in diabetes. In the UKPDS trial, a reduction in

systolic blood pressure from 154 mmHg to 144 mmHg was correlated with a 30% reduction in microalbuminuria[27]. Inhibition of the renin–angiotensin–aldosterone system (RAAS) using angiotensin-converting enzyme inhibitors (ACEIs) and angiotensin II receptor blockers (ARBs) can achieve better renoprotective efficacy compared to other therapeutics despite a similar degree of blood pressure reduction[28,29]. The Irbesartan in Diabetic Nephropathy Trial demonstrated that patients receiving irbesartan (an ARB) had less incidence of renal replacement therapy (RRT) compared with those receiving amlodipine (a calcium channel blocker)[30]. A recent study suggested that the combination of ACEIs and ARBs, or with other RAAS inhibitors such as aldosterone receptor antagonists, resulted in more effective blood pressure control and a delay in renal function decline[31]. However, the combination of ACEIs and ARBs is not recommended in common practice due to the potential adverse effects, including hyperkalemia and acute renal injury[32]. Another recent addition to the RAAS repertoire is the nonsteroidal mineralocorticoid receptor antagonists, such as finerenone. The combined FIDELIO-/FIGARO-DKD studies showed finerenone significantly reduced the cardiovascular and kidney outcomes across the spectrum of CKD in type 2 diabetes[33].

1.3.2.2 Hyperglycemia and Blood Glucose Control

Hyperglycemia is another important risk factor. It is worth noticing that even in the absence of chronic hyperglycaemia, transient hyperglycaemia/hypoglycaemia, or increased glycaemic variability around a normal average, might have long-term effects on the development and progression of renal complications, suggesting the importance of long-term intensive glucose control. Additionally, many clinical observations revealed that intensive control exhibited the persistent renal benefits compared to short-term and

intermediate-term trails[34–36]. For instance, a study of 11,140 patients with type 2 diabetes reported that fewer patients required RRT compared to the control group after the intensification of glucose control[37]. However, intensive glucose control may render severe hypoglycemia regardless of renal benefits, suggesting that careful precision prescribing and monitoring are necessary in long-term management. Interestingly, some novel glucose-lowering agents displayed renoprotection through mechanisms that are independent of hypoglycemic effects. Particularly, the sodium glucose co-transporter-2 (SGLT2) inhibitors have demonstrated consistent benefits in modifying risks of kidney disease progression in patients with type 2 diabetes, or chronic kidney disease of diverse etiology[38]. In addition, GLP-1 receptor agonists also demonstrated a significantly reduced risk of adverse renal outcomes, including macroalbuminuria, doubling of serum creatinine, end-stage renal disease, and mortality due to nephropathy[39]. But these effects are likely due to other mechanisms such as the suppression of oxidative stress and inflammatory responses, improvement of vascular endothelial function, prevention of renal scarring, facilitation of urinary sodium excretion, and improvement of renal hemodynamics[40,41].

1.3.2.3 Dyslipidemia and Blood Lipid Control

It has been reported that disruption of lipid profiles, including elevated triglycerides, low-density lipoprotein (LDL) cholesterol, apolipoprotein-B-100, or low high-density lipoprotein (HDL) cholesterol levels, are independently correlated with the development of CKD in both type 1 and type 2 diabetes[42,43]. Although lipid-lowering treatment is commonly recommended in CKD patients to mitigate cardiovascular risk and related mortality, whether this practice also benefits the kidneys remains controversial. During 4.8 years of follow-up, there was no significant difference in the incidence of ESRD between

CKD patients receiving simvastatin plus ezetimibe and placebo, in spite of a lower average LDL cholesterol[44]. Further investigation is needed to understand the efficacy of lipid-lowering agents on renal function improvement.

1.3.3 Cardiorenal Interaction

It is widely observed that patients with CKD have an increased risk for cardiovascular disease (CVD) as both conditions share common risk factors. A meta-analysis of 102 prospective studies showed that individuals with type 2 diabetes have a two-fold higher risk for coronary heart disease, stroke, and death resulting from other vascular causes[45]. An analysis performed by the Cardiovascular Health Study revealed that elevated serum creatinine is a significant predictor for CVD, heart failure (HF), cardiovascular- and all-cause mortality[46]. Conversely, subjects with HF also have more than two-fold higher risk of CKD and rapid estimated glomerular filtration rate (eGFR) decline[47]. Together, the epidemiological evidence supports the bidirectional link between the kidney and heart, with dysfunction in one organ may trigger disease progression in the other organ.

1.3.4 Challenges and Future Perspectives

Although significant advances have been made in the screening and management of DKD, challenges remain as the underlying mechanisms are not fully understood. Urinary albumin is currently the most important criterion for staging of DKD, but many patients with diabetes and renal impairment do not show excessive albuminuria. Likewise, patients with microalbuminuria do not develop into macroalbuminuria as in the classic paradigm. The advance of intensive management of diabetes, including control of hyperglycemia and hypertension, has greatly reduced the incidence of progression of CKD. Nevertheless, some

studies showed that renal end points such as ESKD are not prevented, and treatment often comes with considerable pill burden and expense. It is still necessary to explore novel therapies to potentially delay, halt, and restore the progression of DKD[48].

1.4 Insulin-like Growth Factor Binding Protein 7 (IGFBP7)

Insulin-like growth factor (IGF) binding protein family (IGFBPs) was initially described as a group of regulatory proteins of IGFs within the circulation, mainly regulating the bioavailability and tissue accessibility of IGFs[49]. Specifically, IGFBPs can regulate the activity of IGF signalling pathway by modulating the half-life and access of IGFs to their receptors, thus regulating a series of biological processes, including cell growth, proliferation, and apoptosis[50–52]. IGFBPs consist of three domains: the N-terminal domain, the C-terminal domain, and the central domain. Both N-terminal and C-terminal domains contain conserved cysteine residues. The N-terminal domain contains a common IGFBP motif responsible for IGFs binding[53], while the C-terminal domain is variable among different members of the IGFBP family[54]. The central domain is structurally different from other domains and contains glycosylation and phosphorylation sites, which can affect the activity and stability of IGFBPs[55]. IGFBP7, also known as IGFBP-rP1, AGM, T1A12, TAF, mac25, and PSF, is a glycoprotein of approximately 30 kDa that belongs to this superfamily[56]. Despite its widespread presence in multiple organs, it is most highly expressed in the kidneys, heart, and brain[57]. Unlike IGFBP1-6, IGFBP7 has a lower affinity to IGFs. It has a 100-fold lower affinity for binding to IGF-1 but has a strong affinity with insulin[58]. Therefore, it is believed to have various physiologic and pathologic functions in an IGF-independent manner[59]. Previous studies showed that IGFBP7 was involved in tumor development as a tumor suppressor and regulated multiple biological processes,

including cell proliferation, cell adhesion, apoptosis, cellular senescence, and angiogenesis[60–63].

1.4.1 IGFBP7 as a Cardiac Injury Marker

IGFBP7 was first described to indicate diastolic dysfunction in heart failure with reduced ejection fraction (HFrEF). In Gandhi's study, elevated baseline IGFBP7 concentration was not correlated with left ventricular size, left ventricular volumes, and systolic function (ejection fraction), but significantly associated with diastolic dysfunction, such as left atrial volume index (LAVi), transmitral E/A ratio, E/E' ratio, and right ventricular systolic pressure (RVSP). The highest percentage of patients with E/A>1.5 also expressed the highest tertile of IGFBP7 concentration. NT-proBNP was not significantly correlated with IGFBP7 in adjusted analyses, indicating independent biological pathways of activation. Compared with other biomarkers, only IGFBP7 was significantly associated with diastolic parameters[64]. IGFBP7 also revealed excellent prognostic performance in HFrEF patients. Considering IGFBP7 as a continuous variable, IGFBP7 level was linearly and positively correlated with the risk of different cardiac outcomes, including the primary composite endpoint, hospitalization or urgent visit for heart failure, death from cardiovascular cause, and death from any cause. Specifically, the adjusted hazard ratio for the primary endpoint in tertile 3 was 1.48 compared to tertile 1. At 1 year, patients with an increase in IGFBP7 of more than 30 ng/mL had a higher risk of HF hospitalization, cardiovascular death, and all-cause death compared with patients with less increase in IGFBP7 levels[65].

Based on the prognostication of diastolic function, IGFBP7 was applied more broadly in heart failure with preserved ejection fraction (HFpEF), another distinct type of

HF known to feature diastolic dysfunction. Serum IGFBP7 levels significantly increased with the severity of cardiac dysfunction, from controls to asymptomatic left ventricular diastolic dysfunction to HFpEF, whereas IGF-1 levels gradually declined[66]. Patients with IGFBP7/IGF-1 ratios above the median exhibited significantly higher LAVi, E/E' ratio, and NT-proBNP levels compared to those below the median. It is worth noticing that the IGFBP7/IGF-1 ratios were significantly higher in diabetes patients, suggesting the association between IGFBP7 levels and the risk of metabolic syndrome[66]. In another study, patients with higher baseline IGFBP7 concentrations were older with more complications, such as atrial fibrillation and congestion, as well as having significantly higher cystatin C, NT-proBNP, pro-collagen type III amino-terminal peptide (PIIINP), highly sensitive troponin I (hsTnI), and galectin-3 concentrations. Elevated baseline IGFBP7 was inversely correlated with peak oxygen consumption (VO_{2max}), an indicator of cardiac function capacity. Treatment of sildenafil for 24 weeks successfully prevented the elevation of IGFBP7 compared to placebo[67]. Similar to previous studies, higher baseline IGFBP7 suggested increased LA width, LAVi, E/A ratio, and E/E' ratio. Individuals with higher baseline LAVi had higher concentrations of both IGFBP7 and NT-proBNP[68]. IGFBP7 revealed a strong prediction of cardiac outcomes in both HFrEF and HFpEF patients. Higher plasma IGFBP7 concentrations were significantly associated with a higher risk of three main endpoints (hospitalization, all-cause mortality, and combined hospitalization and mortality) after 21 months[69].

During a study of 8.4 years of follow-up, higher IGFBP7 levels strongly indicated a higher cumulative incidence of HF. The absolute risk of incident HF was 8.92% in the highest tertile group. Changes in IGFBP7 levels were also significantly associated with risk

for incident HF, that a 10% relative increase in IGFBP7 levels was correlated with a 15% increase in the risk of incident HF. The prediction effect of baseline and change of IGFBP7 levels on incident HF was independent of NT-proBNP level[70]. Plasma IGFBP7 level was significantly higher in HF patients compared to healthy controls, and decreased after heart transplantation, matching the control's level. There was also a significant correlation between the change in IGFBP7 level and changes in mean right atrial pressure and NT-proBNP[71].

Hage et al. compared the association of cardiac outcomes using serum IGFBP7 in HFrEF and HFpEF[72]. In HFpEF, IGFBP7 was significantly linked with diastolic dysfunction, indicated by E/A ratio and E/E' ratio. In HFrEF, IGFBP7 was significantly correlated with age, atrial fibrillation, and other cardiac biomarkers such as MR-pro-adrenomedullin, indicating the severity of HF. More importantly, the prognostic value of IGFBP7 was only significant in HFpEF but not in HFrEF, suggesting distinct pathophysiological contributions of IGFBP7 across heart failure subtypes.

In both coronary artery disease (CAD) and acute myocardial infarction (MI) groups, IGFBP7 levels were significantly higher compared to the healthy controls, but were not significantly changed during hospitalization in MI patients. No significant correlation between IGFBP7 concentration and the extent of coronary lesions was found. During a two-year follow-up, no significant difference in IGFBP7 concentration was observed in deaths compared to survivors. There were significant but weak positive correlations between IGFBP7 and other biomarkers, including fibrinogen and creatinine levels[73]. Similarly, IGFBP7 showed significant correlations between kidney function parameters

(creatinine and urea), as well as cardiac injury markers (TnT and NT-proBNP) in ischemic heart disease group[74].

In patients admitted with symptoms of dyspnea, median concentrations of NT-proBNP and IGFBP7 were significantly higher in those diagnosed with acute HF. The sensitivity and specificity values combining NT-proBNP and IGFBP7 were higher than NT-proBNP alone for the diagnosis of acute HF. In patients with NT-proBNP concentrations >300 pg/mL, IGFBP7 correctly helped to reclassify the presence of acute HF. In addition, higher log_2-IGFBP7 predicted death or rehospitalization during 6 months follow up[75].

The details of IGFBP7 as a cardiac injury biomarker is summarized in **Table 1**.

Table 1 Summary of IGFBP7 as a cardiac injury biomarker.

The Association Between IGFBP7 & Cardiac Function/Outcome	The Association Between IGFBP7 & Other Biomarkers	Heart Failure Type	Reference
Elevated baseline IGFBP7 was significantly correlated with diastolic dysfunction such as LAVi, transmitral E/A ratio, E/E' ratio, and RVSP	NT-proBNP was not significantly correlated with IGFBP7	HFrEF	Gandhi et al. (2014)
Linear and positive relationships between level of IGFBP-7 and risk for cardiac outcomes (the primary composite endpoint, hospitalization or urgent visit for HF, death from CV cause, and death from any cause)	Higher baseline IGFBP7 was significantly correlated with higher NT-proBNP, hsTnT, bilirubin, alkaline phosphatase and HbA_{1c}	HFrEF	Adamson et al. (2023)
Patients with higher IGFBP-7/IGF-1 ratios demonstrated significantly higher LAVi and E/E' ratio	IGFBP-7/IGF-1 ratio was positively correlated with NT-proBNP, sST2 and hs-CRP	HFpEF	Barroso et al. (2016)
Higher baseline IGFBP7 was significantly correlated with higher E velocity, E/E' ratio, LAVi, RVSP, and VO_{2max}	IGFBP7 concentration was significantly correlated with cystatin C, NT-proBNP, PIIINP, hsTnI, and galectin-3 levels Baseline NT-proBNP demonstrated correlations with systolic function while IGFBP7 did not	HFpEF	Gandhi et al. (2016)
Higher baseline IGFBP7 was significantly correlated with higher LA width, LAVi, E/A ratio and E/E' ratio	Baseline IGFBP7 was significantly correlated with sST2, MMP2, galectin-3, PIIINP, BNP and NT-proBNP	HFpEF	Januzzi et al. (2018)

	Higher NT-proBNP and IGBFP7 were significantly correlated with higher LAVi		
Higher plasma IGFBP7 concentration was significantly associated with higher risk of hospitalization and mortality endpoints	Higher baseline IGFBP7 level was significantly correlated higher NT-proBNP, hsTnT, GDF-15 and urea	HFrEF & HFpEF	Bracun et al. (2022)
Higher tertiles of baseline IGFBP7 were associated with significantly higher first HF event, total HF event, cardiovascular death, sustained eGFR reduction ≥40% or end-stage renal disease	Higher baseline IGFBP7 was associated with higher albumin/creatinine ratio, NT-proBNP and hs-cTnT	HFrEF & HFpEF	Ferreira et al. (2024)
IGFBP7 correlated with NYHA class in both HFrEF and HFpEF In HFrEF, IGFBP7 correlated with age and atrial fibrillation In HFpEF, IGFBP7 correlated with E/E' ratio and E/A ratio, as well as predicting the cardiac outcome	In HFrEF, IGFBP7 was correlated with NT-proBNP, tumorigenicity 2, leptin, galectin-3, IGFBP-1 and MR-pro-adrenomedullin	HFrEF & HFpEF	Hage et al. (2018)
Higher baseline IGFBP7 level and change in IGFBP7 level were significantly associated with risk for incident HF	Higher baseline IGFBP7 level was significantly correlated with higher baseline NT-proBNP	N/A	Kamar et al. (2024)
Change in IGFBP7 was significantly associated with change in mean right atrial pressure	Change in IGFBP7 was significantly associated with change in NT-proBNP	Dilated cardiomyopathy, ischaemic cardiomyopathy, and hypertrophic cardiomyopathy	Ahmed et al. (2020)

No significant correlation between IGFBP7 and the extent of coronary lesions No change in IGFBP7 concentration during hospitalization in MI patients	IGFBP7 had positive correlations with fibrinogen and creatinine concentrations	CAD & MI	Lisowska et al. (2019)
Ischemic heart disease patients exhibited significantly higher concentrations of IGFBP7 than healthy controls	IGFBP7 had significant positive correlations with creatinine, urea, TnT and NT-proBNP concentrations	Ischemic heart disease	Lisowska et al. (2022)
Addition of IGFBP7 to NT-proBNP significantly improved the specificity and sensitivity of HF diagnosis Higher log_2-IGFBP7 concentration predicted death or rehospitalization at 6 months	A modest correlation between IGFBP7, NT-proBNP, and hsTnT in all patients and patients with acute HF	Acute HF	Ibrahim et al. (2020)

1.4.2 IGFBP7 as a Kidney Injury Marker

Apart from cardiac events, many studies investigating cardiac dysfunction also suggested that IGFBP7 could reflect renal function. In HFpEF, a change in eGFR was significantly correlated with a change in IGFBP7, suggesting that IGFBP7 can indicate renal function change[67]. In different ejection fraction spectrum, higher tertiles of IGFBP7 were significantly associated with higher risk of renal composite endpoints (sustained eGFR reduction$\geqslant$40% or ESRD)[76].

The diagnostic performance of IGFBP7 as a biomarker of acute kidney injury (AKI) was first described in the Sapphire study. Together with another cell cycle arrest biomarker called tissue inhibitor of metalloproteinases-2 (TIMP-2), urinary [TIMP-2]·[IGFBP7] revealed significantly better risk stratification and sensitivity compared to all previously described markers of AKI, with the area under the curve (AUC) of 0.80[77]. It was further validated that the sensitivity of urinary [TIMP-2]·[IGFBP7] to identify critically ill patients at high risk for moderate to severe AKI within 12 h can be as high as 92% (at the 0.3 cutoff level). Specifically, patients with urinary [TIMP-2]·[IGFBP7] greater than 0.3 had seven times the risk for AKI[78]. Another study proved that the predictive ability of [TIMP-2]·[IGFBP7] was the best for severe AKI within 12 h, and can last until 7 days[79]. Therefore, in 2014, [TIMP-2]·[IGFBP7] test was approved by the FDA for risk assessment of AKI in ICU patients[80].

Patients with acute cardiac injury are often reported to have an increased risk for AKI. Therefore, it has been proposed that urinary [TIMP-2]·[IGFBP7] testing should be applied within the first 72 h of ICU admission in patients at risk for AKI, including those with unstable hemodynamics after cardiovascular surgery or cardiac arrest[81]. It has been

reported in several studies that diagnosis based on [TIMP-2]·[IGFBP7] can be much earlier than other canonical biomarkers, such as creatinine. In Meersch's study, urinary [TIMP-2]·[IGFBP7] yielded good sensitivity and specificity for AKI at 4 h after cardiopulmonary bypass surgery (cutoff=0.3), whereas diagnosis using serum creatinine did not work until 1–3 days post surgery[82]. Similarly, urinary [TIMP-2]·[IGFBP7] significantly increased 4 h after coronary artery bypass surgery in patients with AKI stage 2 or 3, while serum creatinine did not increase until 48 h. At 4 h after the surgery, [TIMP-2]·[IGFBP7] had higher diagnostic accuracy than serum creatinine (AUC=0.861 and 0.362, respectively)[83].

In patients with out-of-hospital cardiac arrest (OHCA), urinary [TIMP-2]·[IGFBP7] was superior to other biomarkers, including serum creatinine, urea, and cystatin C. The noticeable elevation of [TIMP-2]·[IGFBP7] in those with AKI can be traced back to 3 h after determination of OHCA (AUC=0.97), while other biomarkers showed no significant differences. Patients with stage 3 AKI showed constantly higher [TIMP-2]·[IGFBP7] concentrations compared with those with stage 1 AKI at 3 h and 24 h. It is worth noticing that [TIMP-2]·[IGFBP7] concentration at 24 h measurement also predicted the need for RRT (AUC=0.78), revealing a promising prognostic value[84]. With the excellent performance of AKI prediction, combining [TIMP-2]·[IGFBP7], serum creatinine, and urine output in a multivariable model was significantly more predictive than serum creatinine or urine output values alone[85].

IGFBP7 also successfully predicted cardiac and renal complications following cardiac surgery, with a higher predictive value compared to other biomarkers. For congestive acute kidney injury, defined by AKI in the presence of right ventricular failure, IGFBP7 had a significantly higher adjusted AUC than NT-proBNP (AUC=0.90 and 0.87,

respectively). For each 10 ng/mL increase in IGFBP7, the adjusted odds ratio would be 1.97 for congestive acute kidney injury[86]. A meta-analysis of 20 studies with 3625 patients proved that [TIMP-2]·[IGFBP7] is reliable for the prediction of all-cause AKI, and the estimated sensitivity of all-cause AKI was 0.79[87]. In summary, IGFBP7 exhibited distinguishing performance in diagnostic and predictive ability for AKI.

Apart from short-term prediction for AKI, new evidence shows that serum IGFBP7 levels can also be used to predict renal dysfunction over long duration. In the Canagliflozin Cardiovascular Assessment Study (CANVAS) Program, among a population of patients with type 2 diabetes and at risk for DKD, higher baseline IGFBP7 was significantly associated with a reduction in eGFR, need for RRT, and the composite renal endpoint plus cardiovascular death. Interestingly, higher IGFBP7 concentration at 1 year had an even stronger prediction of the composite renal endpoint[88]. Given its prognostication for the development and progression of renal dysfunction, IGFBP7 is so far the best biomarker for both acute and chronic renal injury.

1.4.3 The Role of IGFBP7 in Cardiac and Renal Deficiency

1.4.3.1 The Role of IGFBP7 in Cardiac Deficiency

Although IGFBP7 is recognized as a promising biomarker for cardiac and renal injury, the underlying mechanisms by which it is released in cardiac and renal dysfunction are still elusive. Whether IGFBP7 is a mere biomarker, or a biomediator is still being explored. IGFBP7 is believed to have either pro-angiogenic or anti-angiogenic effects in physiological angiogenesis, depending on its surrounding microenvironment[89]. But current studies in cardiac and renal remodelling indicated that chronic elevation of IGFBP7 is generally associated with worse outcomes.

In 2022, our lab reported that IGFBP7 is not only a biomarker for HFpEF but also directly regulates pathological cardiac remodeling, senescence, and fibrosis by suppressing the FOXO3a-mediated pro-longevity pathway, thereby accelerating the progression of heart failure. In a heart failure mouse model induced by pressure overload, IGFBP7 was significantly elevated in both serum and heart. Moreover, this detrimental effect can be reduced by antibody neutralization of IGFBP7 or cardiac-specific IGFBP7 ablation via AAV9, suggesting that IGFBP7 can be used as a therapeutic target for chronological age-related diseases[90]. Another study elucidated that the knockout of *high-temperature requirement A serine peptidase 3 (Htra3)*, a suppressor of transforming growth factor-β (TGF-β) signaling pathway in cardiac fibroblasts, led to cardiac dysfunction induced by pressure overload. The activation of TGF-β signaling was accompanied by the release of secretory proteins (e.g. IGFBP7) from the failing cardiomyocytes, suggesting that the Htra3-TGF-β-IGFBP7 axis can be used as a novel therapeutic target for heart failure[91]. Endothelial-specific knockout of IGFBP7 and a vaccine against IGFBP7 significantly improved cardiac function after pressure overload surgery in mice. Single-cell RNA-seq of cardiomyocytes showed that oxidative phosphorylation related gene expression and metabolites were significantly upregulated in endothelial-specific *Igfbp7* knockout mice. Also, the expression of IGFBP7 was significantly enriched in heart failure patient biopsy samples compared to controls. Taken together, these results indicated that IGFBP7 was mainly derived from endothelial cells during cardiac remodeling, and it adversely affected cardiac function through the acceleration of cardiomyocyte senescence[92].

1.4.3.2 The Role and Localization of IGFBP7 in Renal Deficiency

Studies to date show that IGFBP7 is upregulated in AKI, and decreasing IGFBP7 level significantly improves renal phenotypes. Yu et al. indicated that serum, urine, and tissue expression levels of IGFBP7 were greatly increased in AKI patients, as well as AKI mouse model induced by cisplatin and ischemia–reperfusion injury[93]. However, according to their study, IGFBP7 was mainly localized in the renal tubules in murine model of AKI. Loss of IGFBP7 protected against AKI by reducing KIM1 and inflammatory cytokine production, inhibiting NF-κB activation, ameliorating programmed cell death, and promoting kidney repair and regeneration. Conditional knockout of IGFBP7 in the proximal tubules obtained similar protective effects as global knockout against AKI, further suggesting that tubular epithelial cells may be the main production sites of IGFBP7. IGFBP7 was shown to interact with poly [ADP-ribose] polymerase 1 (PARP1) and inhibit its polyubiquitination by antagonizing the E3 ubiquitin ligase ring finger protein 4 (RNF4). In 2025, the same group reported that knockout or proximal tubule-specific knockout of IGFBP7 significantly attenuated renal fibrosis in several kidney injury mouse models[94]. Mechanistically, they found that IGFBP7 induced mesenchymal phenotypes, possibly through promoting the dimerization, acetylation, and nuclear translocation of pyruvate kinase M2 (PKM2). PKM2 subsequently inhibited the ubiquitination of lipogenic transcription factor SREBP1, promoting lipogenesis and lipid accumulation.

In cultured human renal proximal epithelial cells, IGFBP7 was found to be upregulated by the activation of TGF-β1 in a dose and time-dependent manner. The activation of IGFBP7 is achieved through Smad2/4 mediated pathway, but not MAPK pathways. In patients with overt DKD, IGFBP7 was colocalized with TGF-β1 in the proximal tubules, while no trace of IGFBP7 was observed in glomerular cells[95]. Several

cell markers of proximal tubules confirmed that IGFBP7 was predominantly expressed in proximal tubules rather than distal tubules, and strong protein expression of IGFBP7 was found in the luminal brush-border region of a subset of proximal tubule cells[96]. In contrast, another study indicated that IGFBP7 was detected in both glomeruli and tubules in AKI biopsies, and glomerulosclerosis score and tubular injury score were positively correlated with the levels of IGFBP7 in glomeruli and tubules, respectively. In addition to localizing in megalin-positive proximal tubules, IGFBP7 was indicated to be in a few podocytes, but not mesangial cells and endothelial cells in the glomerulus of again AKI tissues[97].

1.5 Mouse Models of Diabetic Kidney Disease

Mice are widely used in biomedical research because of their relatively low cost, fecundity, short gestation times, and practicability for genetic manipulation. However, most of the mouse models for DKD only manifest modest kidney abnormality features, suggesting the importance of careful model selection[98]. The Animal Models of Diabetic Complications Consortium established key criteria for ideal rodent models of DKD based on clinical diagnostic and pathological findings. An ideal mouse model should include functional and pathological characteristics, including at least a 10-fold increase in albuminuria, systemic hypertension, advanced mesangial matrix expansion with or without nodular sclerosis and mesangiolysis, any degree of arteriolar hyalinosis, and tubulointerstitial fibrosis[98,99].

Streptozotocin (STZ) is a selective pancreatic islet β-cell-cytotoxic agent that is commonly used to induce β-cell necrosis and diabetes[100]. The main advantage is that it can be applied to any pre-existing model to induce diabetes. TTRhRen (Transthyretin Human Renin) mice also known as Lin3 mice, are a genetically modified mouse model that

overexpresses human renin in the liver, leading to chronic, angiotensin II-dependent hypertension and cardiac hypertrophy by 10-12 weeks of age[101]. Hypertensive Lin3 mice, combined with 5-day intraperitoneal STZ injection, recapitulate key features of human DKD, including dramatic increase of albuminuria, glomerular hypertrophy and scarring, and tubulointerstitial fibrosis[102]. Compared to another DKD mouse model with similar histopathological phenotypes (induced by genetic deficiency of eNOS on the *db/db* background)[103], Lin3+STZ is simpler to execute (requires less complicated breeding scheme), more reproducible, incurs shorter time frame. Thus, the Lin3+STZ model is used in this study, considering a robust phenotypic profile and easier breeding schemes.

1.6 Rationale, Objective, Hypothesis & Aims

We recognize that IGFBP7 is an excellent biomarker for heart and kidney impairment, but the role of IGFBP7 in the DKD setting is completely unknown. According to previous studies, it is possible that IGFBP7 would be highly upregulated in DKD, contributing to potential kidney-heart crosstalk and dysfunction in both organs. The purpose of this thesis is to set the stage for more in-depth studies, more specifically, to investigate the expression and localization of IGFBP7 in diabetic kidney and heart, providing clues of its potential beneficial/detrimental role in DKD. Achieving this purpose will be obtained through the following:

Overall aim: determine the level and localization of IGFBP7 in the kidney and heart under the circumstances of DKD. We hypothesize that IGFBP7 will be excessively produced in the kidney and heart in DKD. In the kidney, IGFBP7 is upregulated in the glomeruli and not just around tubules as previously described. The overall aim will be divided into the following sub-aims:

Aim 1: Explore the level and localization of IGFBP7 in the kidney in the DKD mouse model

Aim 2: Assess cardiac functional changes of the DKD mouse model, and the level and localization of IGFBP7 in the heart

2. Materials and Methods

2.1 Generation of Diabetic Kidney Disease Mouse Model

Heterozygous Lin3 males with a FVB genetic background were obtained from Dr. Dylan Burger's Lab, University of Ottawa. Wild-type (WT) FVB females were purchased from Charles River. Trio-breeding scheme was used, and pups were weaned 21 days after birth. All animals were bred and handled in accordance with the animal ethics and protocols of Animal Care Veterinary Services (ACVS) of University of Ottawa (protocol# HIe-4352) and the Canadian Council of Animal Care (CCAC) standards. Animals were housed in identical conditions, provided with *ad libitum* food and water, at the ACVS facility, Faculty of Medicine, University of Ottawa.

At 8-10 weeks of age, Lin3 and WT control male and female mice were randomized to receive either STZ (50 mg Kg^{-1} BW^{-1}) or control (0.1M sodium citrate as vehicle) via intraperitoneal injection for 5 days. Mice were randomly divided into four groups: WT+sodium citrate, WT+STZ, Lin3+sodium citrate, and Lin3+STZ. Induction of diabetes was confirmed two weeks after STZ injection via 6 h fasting glucose and glucose tolerance tests. Briefly, mice were fasted for 6 hours before the test. A fasting (baseline) glucose level was obtained from tail venous blood using glucometers (Roche ACCU-Chek). 1 mg/g body weight glucose was then delivered intraperitoneally, followed by serial blood collection at 15, 30, 45, 60, 90, and 120 minutes post-injection. Mice were followed until 10 weeks post-STZ. At end point, mice were euthanized using CO2 inhalation and perfused with phosphate buffered saline (PBS). Blood was collected through right ventricular cardiac puncture, and the following organs were collected as part of sample collection: heart, lung, liver, kidney, and brain. A detailed procedural timeline is shown in **Figure 3**.

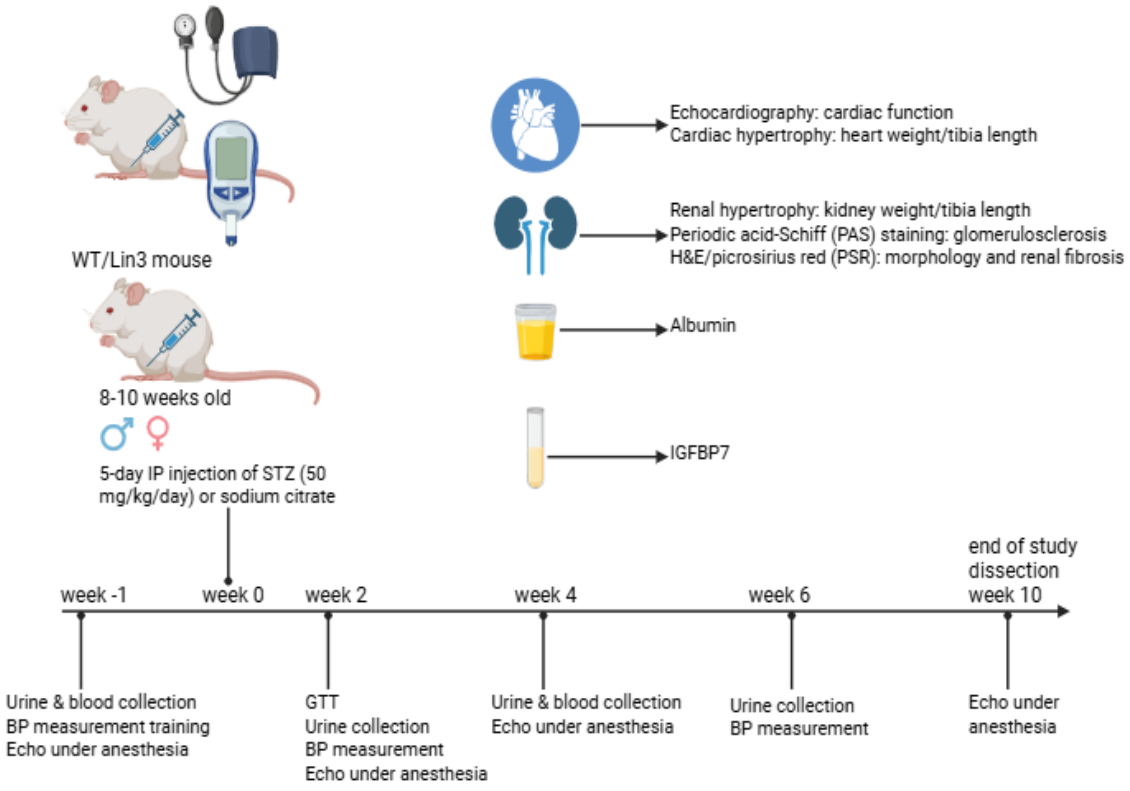

Figure 3 Animal model study timeline. 8-10 weeks old male and female mice were randomized to receive either STZ (50 mg/Kg BW) or control (0.1M sodium citrate) for 5 continuous days. Diabetes was confirmed 2 weeks after STZ injection by fasting glucose and glucose tolerance test. Urine and blood were collected until 10 weeks post-STZ. At week 10, mice were euthanized, and tissues were harvested. Figure was generated using the Biorender platform.

2.2 Blood Pressure Measurement

Systolic blood pressure (BP) was measured via tail-cuff plethysmography (BP 2000, Visitech Systems, Apex, NC). Before the start of the study, mice received training sessions (≥3 days) at the same time each day. Thereafter, daily experimental systolic BP was obtained at the same time each day (5 preliminary, 10 actual BP readings/day). BP that fell beyond ±2SD was excluded for each specimen. Weekly BP was calculated from three continuous daily measurements.

2.3 Measurement of Cardiac Function in Mice

At baseline and 10 weeks post-STZ, cardiac function was assessed via parasternal long axis view (PLAX), parasternal short axis (SAX), tissue Doppler imaging (TDI), and pulse-wave Doppler imaging using Vevo 2100 imaging system (FUJIFILM VisualSonics). Mice were anesthetized with 1–2% (per liter of O_2) isoflurane during the recordings. Qualitative and quantitative measurements were made using Vevo LAB analytic software (FUJIFILM VisualSonics). Diastolic function was assessed by pulsed-wave Doppler imaging of the transmitral filling pattern with the early transmitral filling wave (E-wave) and the late filling wave due to atrial contraction (A-wave). Diastolic function was also assessed by TDI, with the measurement of early diastolic (E′) myocardial velocities. Isovolumic relaxation time (IVRT) was measured as the time from closure of the aortic valve to the initiation of the E-wave. Systolic function (Left Ventricular Ejection Fraction) was estimated by the mean values from PLAX and SAX images. Left ventricle posterior wall thickness at systole and diastole (LVPW;s and LVPW;d) were analyzed using SAX images.

2.4 Enzyme-linked Immunosorbent Assay (ELISA)

Serum samples were obtained from blood samples collected at the time of harvest, by centrifuging at 1,500 xg for 20 minutes at 4 °C and storing at −80 °C until use. Urine samples were collected before sacrifice. Serum IGFBP7 and urine albumin were determined by corresponding ELISA kits (Abcam, ab245712 and ab207620), following manufacturer's protocols. Absorbance was acquired at 450 nm using a Biotek SYNERGY H1 microplate reader, and concentration was calculated from the standard curve.

2.5 Renal Histology

Kidney samples were fixed with 4% paraformaldehyde solution in PBS (PFA, Thermo Fisher Scientific, AAJ19943K2), embedded in paraffin, and sectioned to a thickness of 5 μm. Sections were designated for periodic-acid Schiff (PAS) staining (Sigma-Aldrich, 395B) for histopathology. The stained sections were imaged with a Leica Aperio VERSA 8 slide scanner. Glomerular area was quantified by ImageJ (Fiji), with a minimum of 3 technical replicates and 3 biological replicates.

Glomerulosclerosis was examined on PAS-stained tissues at 400x magnification, in a semi-quantitative manner as described previously[104]. The degree of sclerosis in each glomerulus was subjectively graded on a scale of 1-4: Grade 1, normal or sclerotic area up to 25% (minimal); Grade 2, sclerotic area 25-50% (moderate); Grade 3, sclerotic area 50-75% (moderate to severe), and Grade 4, sclerotic area 75-100% (severe). Grading criteria include mesangial expansion and capillary occlusion. Representative images of different grades are shown in the **Extended Data Figure 1**. A glomerulosclerotic index (GSI) was then calculated using the formula:

$$\mathrm{GSI} = \frac{1 \times \mathrm{N1} + 2 \times \mathrm{N2} + 3 \times \mathrm{N3} + 4 \times \mathrm{N4}}{\mathrm{N1} + \mathrm{N2} + \mathrm{N3} + \mathrm{N4}}$$

Where Nx is the number of glomeruli with each given score for a given section

For each biological replicate, at least 3 sections were randomly selected and analyzed in a blinded manner.

2.6 RNA In Situ Hybridization

After fixing with 4% PFA, kidney tissues went through gradient sucrose from 10% to 30%, embedded with Tissue-Tek® O.C.T. Compound (Sakura), and then sectioned to a thickness of 10 μm. In situ hybridization was applied to explore the transcriptional level and colocalization of *Igfbp7* using RNAscope Multiplex Fluorescent Reagent Kit v2 (ACD Bio). Sections were prepared following the guidance of user manual ("fixed-frozen tissue sample preparation and pretreatment"). Different probes assigned to different channels were applied (ACD Bio, 425741, 507051-C3, 411831-C2, 316721-C2), followed by different concentrations of diluted fluorophores. Images were captured with a Leica Aperio VERSA 8 slide scanner.

2.7 Statistics and Reproducibility

Statistical analyses for all data were conducted using GraphPad Prism version 9 (GraphPad Software). Comparisons between multiple groups of continuous variables were assessed with one-way ANOVA with Tukey's correction for multiple comparisons. Comparisons between multiple groups of continuous variables across different time points were assessed with two-way ANOVA (or mixed model) with Tukey's correction for multiple comparisons. Details of the statistical tests are indicated in the corresponding figure legends. Values are primarily presented as mean ± s.d.; n refers to the sample size. $P < 0.05$ was considered statistically significant a priori. All experiments were repeated

independently with similar results to ensure reproducibility, with specimens collected from two cohorts of subjects.

3. Results

3.1 Validation of the DKD model (hypertension and hyperglycemia)

A significant and constant elevation of BP was observed in both Lin3+sodium citrate and Lin3+STZ male mice at 2- and 6-weeks post STZ injection, compared with WT+sodium citrate group (**Figure 4A**, Lin3+STZ vs. WT+sodium citrate; p=0.0118 and 0.0017 respectively), which confirms that the liver-specific production of human renin drives the chronic hypertension in these mice. Meanwhile, Lin3+sodium citrate and Lin3+STZ showed comparable BP levels at 2- and 6- weeks post STZ (**Figure 4A**, p=0.9849 and 0.9490 respectively), suggesting no superimposed effect of STZ on blood pressure. Similarly, Lin3+STZ females showed significantly higher BP compared to WT+sodium citrate females at both time points (**Figure 4B**, p=0.0345 and <0.0001 respectively). There was a slight increase in BP of Lin3+STZ females, which corresponded with the previous study where STZ mice displayed a slight increase of BP 18 weeks post STZ treatment[102].

Two weeks after STZ injection, a glucose tolerance test was performed to confirm the induction of diabetes. Fasting (baseline) glucose levels at 6 hours were obtained before the delivery of glucose. 1 mg/g body weight glucose was delivered via IP injection, followed by serial blood collection until 120 min post-injection. Both WT+STZ and Lin3+STZ males had significantly higher baseline blood glucose levels compared to their corresponding vehicle-treated groups (**Figure 4C**, p<0.0001), while there was no significant difference between WT+STZ and Lin3+STZ groups (p=0.9936). A similar trend

was observed in female groups, with STZ groups showing significantly higher baseline blood glucose levels compared to sodium citrate-treated groups (**Figure 4D**, p=0.02 and 0.0002). Severe diabetes in mice is usually considered with a 6 h fasting blood glucose concentration from 16.7 to 33.3 mmol/L[100]. Both male and female STZ groups exhibited fasting glucose levels at approximately 20 mmol/L, so we can confirm that diabetes was successfully induced 2 weeks after STZ injection. It is worth noticing that the variations within the group were larger with female STZ groups compared to male STZ groups (s.d.=4.676 in female Lin3+STZ vs. s.d.=2.132 in male Lin3+STZ), suggesting that males are more susceptible to STZ for diabetes induction.

Diabetes was further confirmed by the glucose tolerance test, as diabetic mice will show impaired glucose metabolism and consistently high blood glucose levels after glucose administration. Glucose tolerance curves showed that STZ groups in males and females exhibited significantly higher blood glucose across the whole test (**Figure 4E-F**). Notably, all sodium citrate treated groups reached the peak glucose levels at approximately 30 min after injection, and gradually decreased until 2 h, whereas STZ-treated groups remained constantly high until 2 h, suggesting impaired and prolonged glucose metabolism. At 2 h, both Lin3+STZ males and females showed significantly elevated blood glucose concentrations compared to WT+sodium citrate groups (p=0.0237 and p<0.0001), whereas no significant differences between WT+STZ and Lin3+STZ curves were observed in both sexes. Taken together, the results showed that 5-day STZ administration was sufficient to induce diabetes 2 weeks after STZ exposure, as evidenced by significantly increased fasting blood glucose level and glucose intolerance.

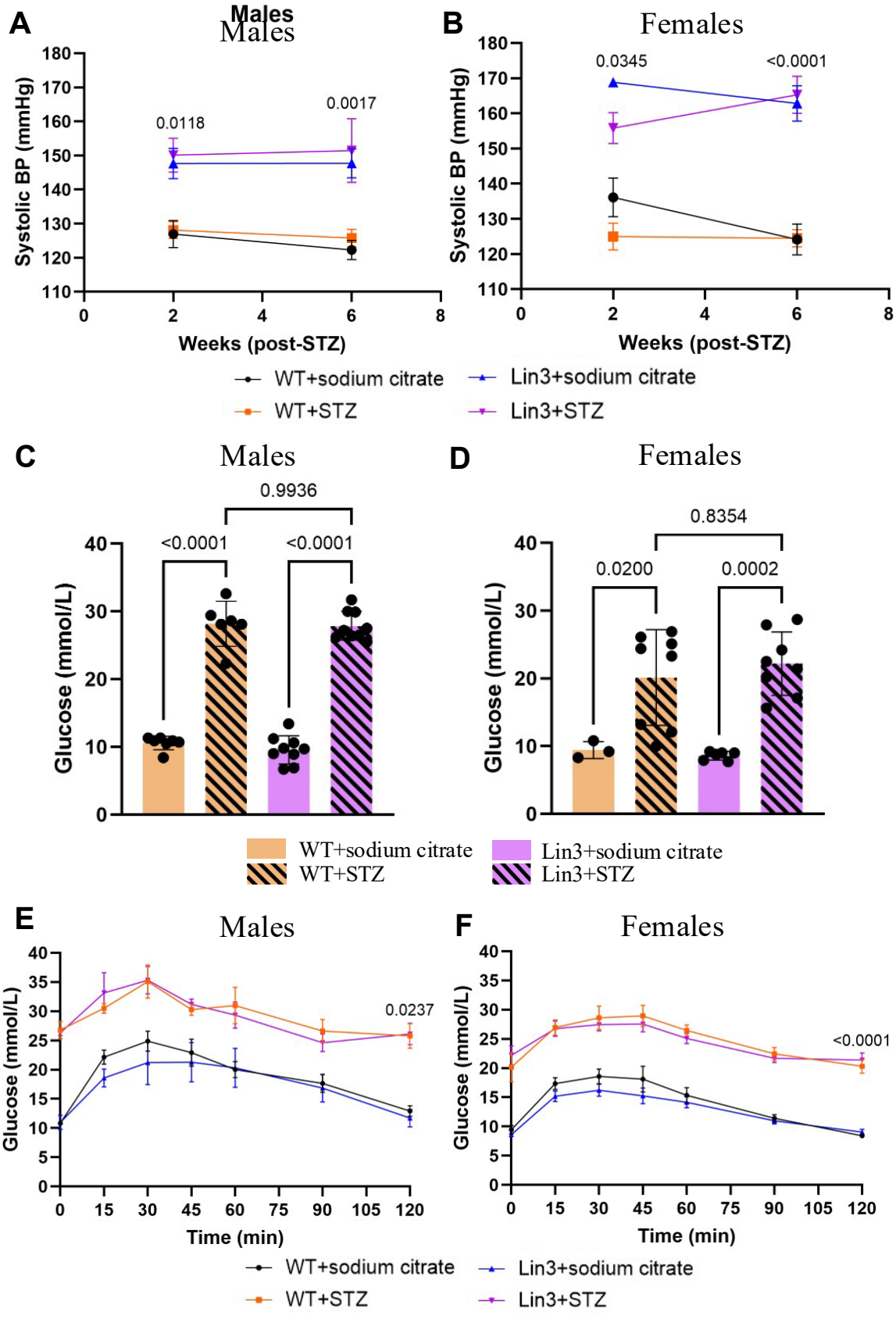
A
Males
Males
Systolic BP (mmHg)
Weeks (post-STZ)
0.0118
0.0017
B
Females
Females
Systolic BP (mmHg)
Weeks (post-STZ)
0.0345
<0.0001
WT+sodium citrate
WT+STZ
Lin3+sodium citrate
Lin3+STZ
C
Males
Glucose (mmol/L)
0.9936
<0.0001
<0.0001
D
Females
Glucose (mmol/L)
0.8354
0.0200
0.0002
WT+sodium citrate
WT+STZ
Lin3+sodium citrate
Lin3+STZ
E
Males
Glucose (mmol/L)
Time (min)
0.0237
F
Females
Glucose (mmol/L)
Time (min)
<0.0001
WT+sodium citrate
WT+STZ
Lin3+sodium citrate
Lin3+STZ

Figure 4 Validation of the DKD model (hypertension and hyperglycemia). (A-B) Systolic BP measured at 2- and 6-weeks post-STZ. Longitudinal BP measurements were obtained by tail-cuff plethysmography in STZ and Lin3 groups (n=2-7 mice per group). Significance was determined using two-way ANOVA (or mixed model) with Tukey's correction. Error bar=s.e.m. (C-D) 6 h fasting glucose level from tail venous blood in males and females. Significant differences were determined using one-way ANOVA with Tukey's correction. Values are presented as mean ± s.d. n=3-9 per treatment group. (E-F) Glucose tolerance curve 2 weeks post STZ injection. A fasting (baseline) glucose level was first obtained from tail venous blood, followed by the IP injection of 1 mg/g body weight glucose. A serial blood collection was performed at 15, 30, 45, 60, 90, and 120 min post-injection. STZ groups in males and females exhibited significantly higher blood glucose during the whole process. There was no significant difference between WT+STZ and Lin3+STZ groups. Male (120 min): Lin3+STZ vs. WT+sodium citrate $p<0.05$; female (120 min): Lin3+STZ vs. WT+sodium citrate $p<0.0001$. Significance was determined using two-way ANOVA (or mixed model) with Tukey's correction. Error bar=s.e.m. n=3-8 per treatment group. $P<0.05$ was considered statistically significant. n refers to the sample size.

3.2 Lin3+STZ males and females developed cardiac and renal hypertrophy

As a preliminary indication of organ damage, key organ weights (heart, kidney, and lung) were measured at sacrifice and normalized to tibia length. In Lin3+sodium citrate males, heart weight was significantly increased compared to WT+sodium citrate (**Figure 5A**, p=0.0182), while there was no significant difference between Lin3+sodium citrate and Lin3+STZ males, indicating that persistent hypertension is the main contributor to cardiac hypertrophy. In contrast, Lin3+STZ males exhibited significant renal hypertrophy compared to Lin3+sodium citrate group (**Figure 5B**, p=0.0025), while WT+STZ and Lin3+STZ groups shared comparable kidney weights, suggesting that kidney remodeling is predominantly affected by STZ treatment rather than hypertension. Cardiac and renal hypertrophy were also observed in females. Lin3+sodium citrate females showed significantly increased heart weight compared to WT+sodium citrate females (**Figure 5D**, p=0.0026), and Lin3+STZ females showed significantly higher kidney weight compared to Lin3+sodium citrate females (**Figure 5E**, p=0.0005). Both males and females did not show significant differences in lung weight among the groups (**Figure 5C and F**), suggesting cardiac hypertrophy at this stage is more a consequence of hypertension, but not reaching the stage of actual heart failure, as heart failure often manifests as pulmonary congestion with increases in lung weight[105].

Overall, the above results were aligned with previous studies, that Lin3 mice show cardiac hypertrophy by the age of 10-12 weeks[101], as well as significant renal hypertrophy in STZ groups[102].

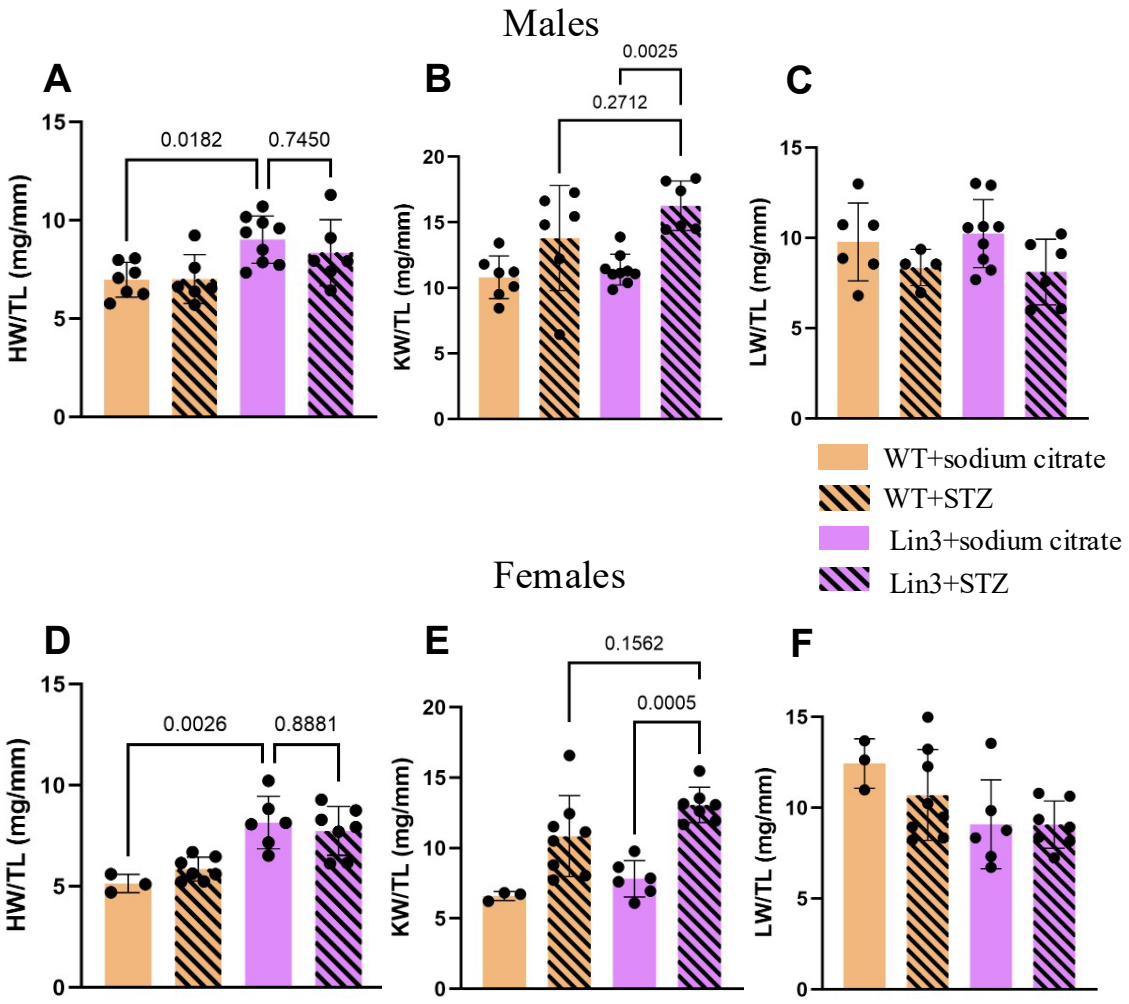

Figure 5 Lin3+STZ males and females developed cardiac and renal hypertrophy at 10 weeks post-STZ. Organ weights (heart, kidney, and lung) were normalized to tibia length for males (A, B, C) and females (D, E, F), respectively. All values are presented as mean ± s.d. n=3-9 per group. $P<0.05$ was considered statistically significant. P values were calculated using one-way ANOVA with Tukey's correction.

3.3 Lin3+STZ males exhibited glomerular hypertrophy, glomerulosclerosis, and albuminuria

PAS staining was applied to further examine the glomerular profiles of kidneys of respective groups. Lin3+STZ males exhibited significant glomerular hypertrophy, represented by increase in glomerular area, compared to WT+sodium citrate group (**Figure 6B**, p=0.0004). The increase of glomerular surface area in Lin3+STZ group was also significant compared to Lin3+sodium citrate (**Figure 6B**, p=0.0008), which is consistent with previous study that showed the combination of hypertension and diabetes yielded exacerbated glomerular hypertrophy than that induced solely by one intervention alone[102]. Lin3+STZ showed advanced glomerulosclerosis compared to WT+sodium citrate, according to the semi-quantitative analysis (**Figure 6C**, p=0.0039), while Lin3+sodium citrate displayed comparable glomerular morphology compared to WT+sodium citrate (**Figure 6C**, p=0.9352). Together with the results in **Figure 5B** and **5E**, it emphasizes that STZ treatment is a more dominant player in the development of renal dysfunction than hypertension. Albuminuria, one of the most important characteristics of DKD, was also observed to be greatly increased in Lin3+STZ (**Figure 6D**). No statistical significance was shown due to the variation within the group caused by the huge sample dilution factor required by the ELISA kit (>8000 times).

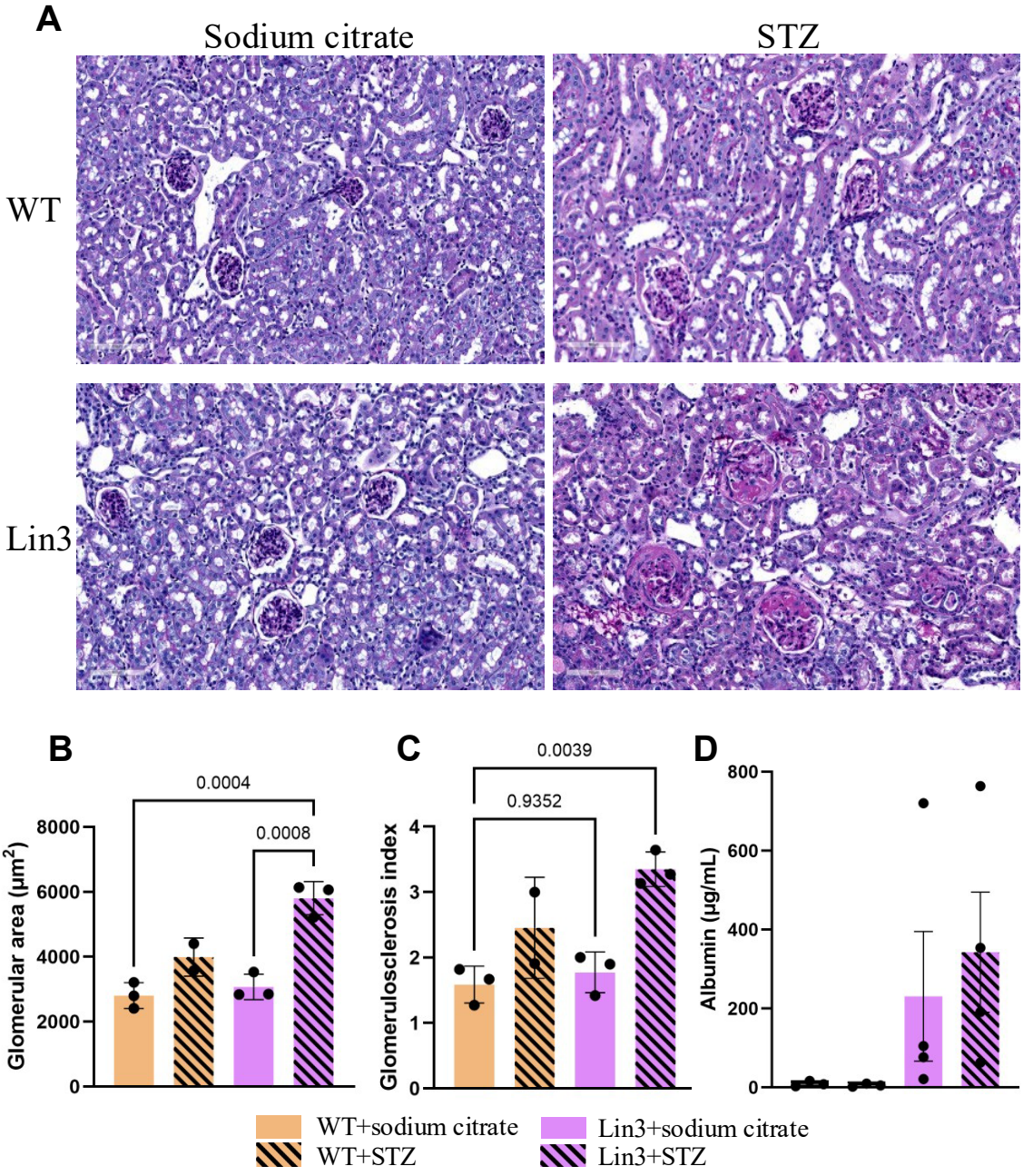

Figure 6 Lin3+STZ males exhibited glomerular hypertrophy, glomerulosclerosis and albuminuria compared to WT+sodium citrate males at 10 weeks post STZ. (A) Representative images of PAS staining of 5 µm thick paraffin kidney cross sections acquired from males. Scale bar=100 µm. (B) Glomerular area analysis was performed on more than 9 glomeruli per mouse using ImageJ, 2-3 mice per group. (C) Semi-quantitative analysis of the degree of glomerulosclerosis. 3 sections with 9-15 glomeruli were included for each mouse, 2-3 mice per group. (D) Urinary albumin levels were measured in urine samples collected at endpoint using an ELISA-based method. n=3-4 per group. All values are presented as mean ± s.d. $P<0.05$ was considered statistically significant. P values were calculated using one-way ANOVA with Tukey's correction. n refers to the sample size.

3.4 Igfbp7 was upregulated in kidney and serum in Lin3+STZ males

We then performed in situ hybridization to determine the transcriptional level of Igfbp7. Unexpectedly, we found that *Igfbp7* was significantly upregulated and accumulated in the glomeruli of Lin3+STZ kidney (**Figure 7A**), rather than tubules as previously described[93,94,96]. Upregulated serum Igfbp7 concentrations were also detected in Lin3+STZ males but not females (**Figure 7B**, p=0.0008).

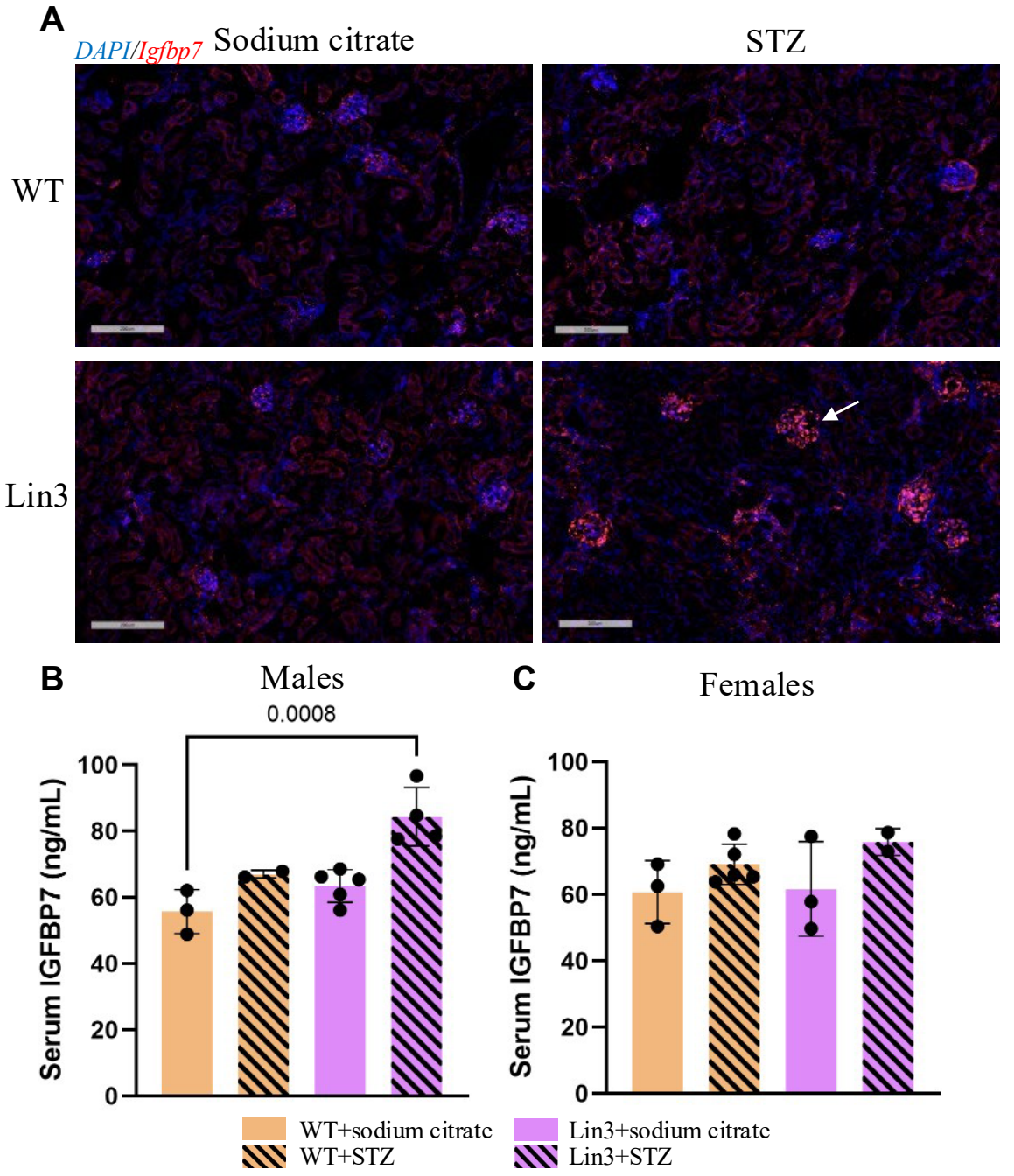

Figure 7 The upregulation of Igfbp7 levels in kidney tissue and serum in males at 10 weeks post-STZ. (A) Transcriptional level of Igfbp7 was determined using RNA in situ hybridization. Scale bar=200 μm. *Igfbp7* was significantly upregulated in the glomeruli instead of tubules in the kidney. (B) Elevated serum Igfbp7 was also evidenced in Lin3+STZ males by ELISA. n=2-5 per group. All values are presented as mean ± s.d.; n refers to the sample size. P<0.05 was considered statistically significant. P values were calculated using one-way ANOVA with Tukey's correction.

3.5 *Igfbp7* was coexpressed with pericyte and podocyte markers but not endothelial cell marker

To determine the spatial localization of IGFBP7 at the cellular level, in situ hybridization was applied for spatial *Igfbp7* gene expression analysis in kidney. Specifically, *Igfbp7* gene expression was visualized together with cell surface specific marker: *Pecam-1* (endothelium); *Pdgfrβ* (pericytes) and *Nphs2* (podocytes). Surprisingly, *Igfbp7* was coexpressed with *Pdgfrβ* and *Nphs2* but not with *Pecam-1* (**Figure 8A-C**), which is different from previous reports that IGFBP7 is mainly expressed in endothelial cells and regulates endothelial activities such as promoting endothelial tube formation and cell adhesion[89]. However, we also recognize that pericytes and mesangial cells may share some common markers such as *Pdgfrβ*. Thus, further investigation including applying more key markers (e.g. PDGFRα and GATA3) or single cell transcriptomic analysis may help us to better distinguish between pericytes and mesangial cells.

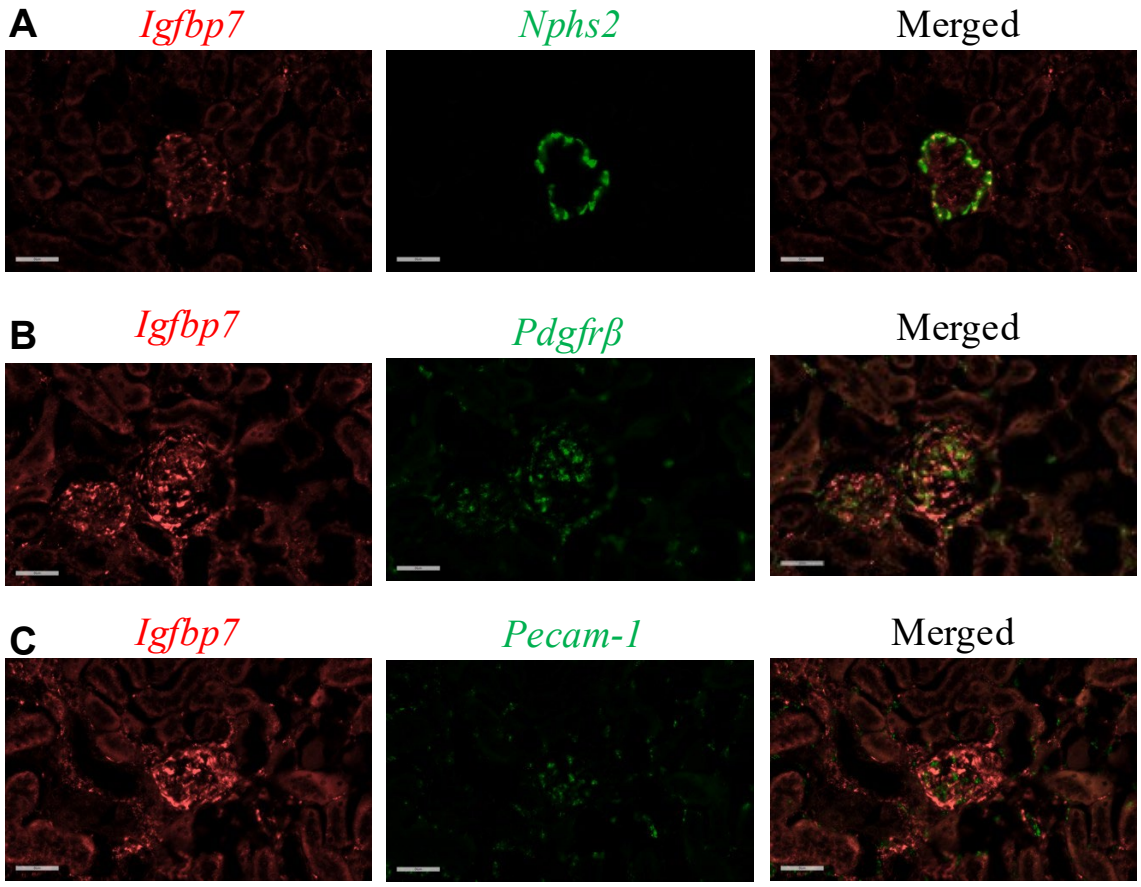

Figure 8 The localization of Igfbp7 in the kidney. Transcriptional level of Igfbp7 was determined using RNA in situ hybridization, combined with different cell markers. Single-stain micrographs are shown along with two-colors merged micrographs to identify colocalization. Scale bar=50 μm. (A) *Igfbp7* (red) was coexpressed with podocyte marker *Nphs2* (green). (B) *Igfbp7* (red) was coexpressed with pericyte marker *Pdgfrβ* (green). (C) *Igfbp7* (red) was not coexpressed with endothelial cell marker *Pecam-1* (green).

3.6 Lin3 males exhibited selected cardiac functional changes

Echocardiography was performed at 10 weeks post-STZ before the harvest to assess the cardiac functional changes. In males, STZ injection significantly increased ejection fraction in Lin3+STZ group compared to Lin3+sodium citrate group (**Figure 9A**, p=0.0001). However, cardiac output was not significantly different across the groups, suggesting the increase in ejection fraction in Lin3+STZ may be a compensatory mechanism for lower heart rate (**Extended Data Figure 2**). In females, there was no significant difference in ejection fraction across the groups (**Figure 10A**). Lin3+sodium citrate males exhibited significantly higher LVPW;s and LVPW;d compared to WT+sodium citrate (**Figure 9B-C**, p=0.0062 and 0.0072, respectively), suggesting an effect of hypertension on increasing left ventricle wall thickness. Lin3+sodium citrate males also showed significantly increased isovolumic relaxation time (IVRT) compared to WT+STZ (**Figure 9D**, p=0.0302), suggesting a sign of diastolic dysfunction caused by hypertension. But other indicators of diastolic dysfunction, such as E/E' ratio that represents left ventricular filling pressure, E/A ratio that represents early to late ventricular filling velocities, did not show any significant changes in different male groups (**Figure 9E-F**). Females, on the other hand, did not show any signs of cardiac functional changes (**Figure 10A-F**). Therefore, we can conclude from this sample that the cardiac functional changes in Lin3+STZ model were present albeit subtle, consistent with the concept that DKD and cardiovascular diseases share some common risk factors, including hypertension and diabetes.

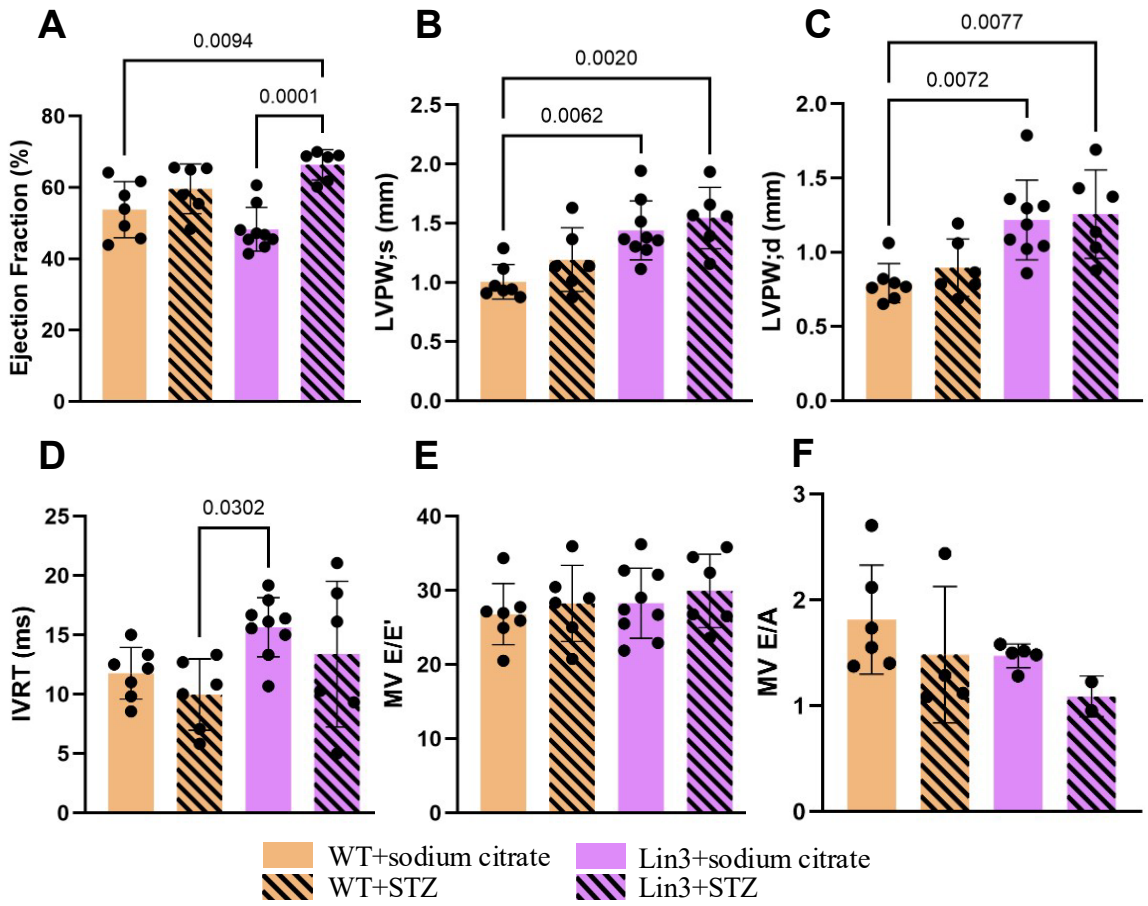

Figure 9 Male cardiac function evaluated by echocardiography at 10 weeks post-STZ. (A) Lin3+STZ males showed significantly higher ejection fraction compared to WT+sodium citrate and Lin3+sodium citrate. (B-C) Both Lin3+sodium citrate and Lin3+STZ males showed significantly increased left ventricular posterior wall thickness compared to WT+sodium citrate, suggesting the effect of hypertension on left ventricular wall thickness. (D) Lin3+sodium citrate males showed significantly prolonged IVRT compared to WT+STZ. (E-F) No significant differences were observed with other indicators of diastolic dysfunction. LVPW;s: end-systolic left ventricular posterior wall thickness. LVPW;d: end-diastolic left ventricular posterior wall thickness. MV E/A: ratio between early and late transmitral filling wave. MV E/E': ratio between mitral E and E′ wave. IVRT: isovolumic relaxation time. All values are presented as mean ± s.d. n=2-9 per group. $P<0.05$ was considered statistically significant. P values were calculated using one-way ANOVA with Tukey's correction.

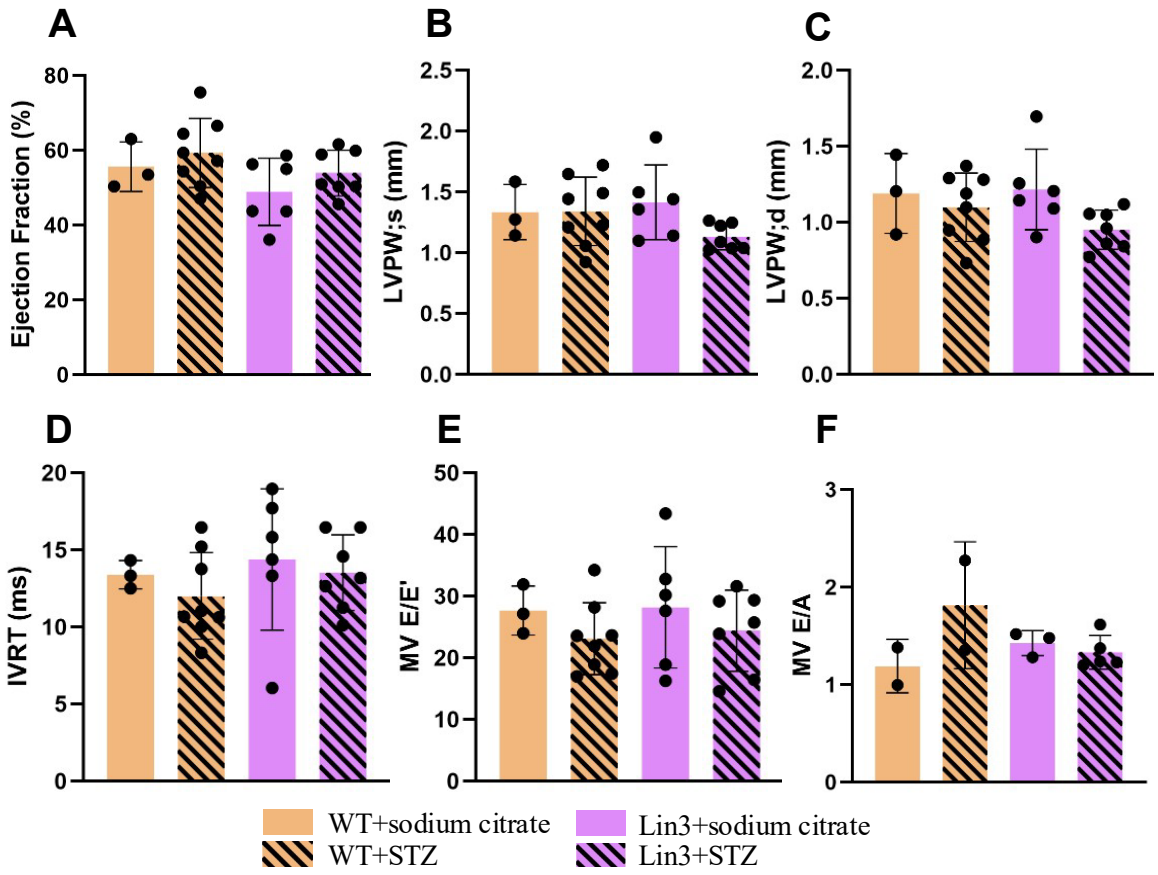

Figure 10 Female cardiac function evaluated by echocardiography at 10 weeks post STZ. No significant signs of cardiac functional changes were observed. LVPW;s: end-systolic left ventricular posterior wall thickness. LVPW;d: end-diastolic left ventricular posterior wall thickness. MV E/A: ratio between early and late transmitral filling wave. MV E/E': ratio between mitral E and E′ wave. IVRT: isovolumic relaxation time. All values are presented as mean ± s.d. n=2-8 per group. $P<0.05$ was considered statistically significant. P values were calculated using one-way ANOVA with Tukey's correction.

3.7 *Igfbp7* was increased surrounding cardiac vasculatures and coexpressed with pericyte marker in Lin3+STZ

Interestingly, although Lin3+STZ mice showed only early cardiac functional changes, the transcriptional level of Igfbp7 in Lin3+STZ heart was noticeably increased compared to WT+sodium citrate, particularly around the cardiac vasculature (**Figure 11A**), suggesting that the elevation of IGFBP7 can happen before the onset of observable cardiac functional changes. Our Lab's previous study indicated that elevated Igfbp7 gene and protein expression in cardiomyocytes of pressure overload HF mouse model[90], but the rise of IGFBP7 levels may be limited to vasculatures at the early stages of pathogenesis. Similar to the kidney, *Igfbp7* was also coexpressed in pericytes featuring positive marker *Pdgfrβ* in the heart (**Figure 11B**).

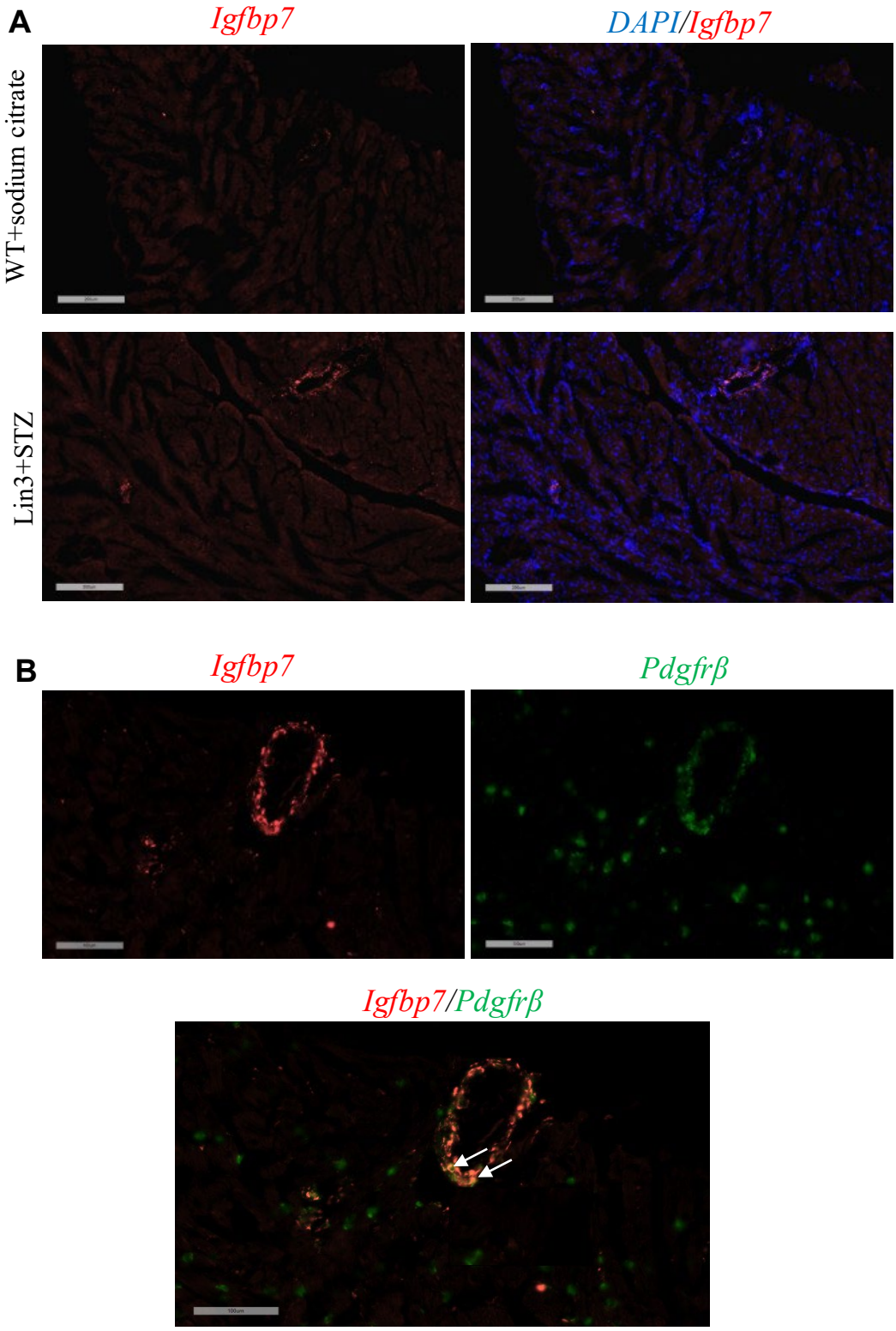

Figure 11 The transcriptional level and localization of Igfbp7 in the heart. Transcriptional level of Igfbp7 was determined by RNA in situ hybridization. (A) *Igfbp7* was elevated in Lin3+STZ males, predominantly around the cardiac vasculatures. Single-stain micrographs are shown along with merged micrographs with *DAPI* to show the nuclei. Scale bar=200 μm. (B) *Igfbp7* (red) was coexpressed with pericyte marker *Pdgfrβ* (green). Scale bar=100 μm.

4. Discussion

4.1 IGFBP7 was elevated in DKD mouse model

IGFBP7 has been widely accepted as an acute kidney injury (AKI) biomarker, but to date there are only a few studies demonstrating IGFBP7's association with chronic renal disease outcomes[88,106]. Our study is the first basic science study to confirm the elevation of IGFBP7 in a DKD mouse model, both in serum and kidney tissues. The results from mice are consistent with the clinical findings, providing a potential scientific explanation that IGFBP7 can be applied as a chronic kidney dysfunction biomarker. This is independent of IGFBP7's diagnostic role in acute kidney injury setting. The Lin3+STZ model, combining hypertension and diabetes, shows key features of DKD, including glomerular hypertrophy, glomerulosclerosis, and albuminuria. It can be a useful tool for us to understand the initiation and progression of DKD.

4.2 IGFBP7 was significantly elevated in glomeruli compared to tubules in DKD

Previous studies reported that IGFBP7 is highly expressed in tubules in human patient biopsies and renal injury mouse models, but all in the context of AKI. This can be explained by the pathophysiogy of acute renal injury, where a combination of reduced renal blood flow and exposure to nephrotoxins render the tubules particularly vulnerable to damage. On the other hand, DKD is commonly considered a glomerular disease, as the reduction of GFR can happen at the early stage of disease. In patients with type 2 diabetes, 54.3% patients have a decline of their eGFR within 3 years, with 30.9% having a decline of more than $-12\,mL/min/1.73m^2$ [108]. Currently used AKI mouse model, including unilateral ureteral obstruction (UUO), ischemia-reperfusion injury (IRI), and cisplatin (CIS) induced renal fibrosis models, are not appropriate to capture the pathophysiology of

chronic DKD. Our study is the first one to reveal the increase of IGFBP7 in glomeruli rather than tubules in chronic DKD, which is the major cause of chronic renal dysfunction, indicating that glomeruli instead are prone to damage from diabetes and IGFBP7 could potentially reflect the extent of glomerular injury.

4.3 IGFBP7 was expressed in podocytes and pericytes rather than endothelial cells in the glomeruli

Pericytes and podocytes are both important for stabilizing microvascular networks and maintaining the glomerular filtration barrier. Pericytes provide physical support, basement membrane integrity and control blood flow for the microvasculature of the glomerulus. Podocytes maintain glomerular filtration by creating a high selective filtration barrier and regulates size through contraction and charge selectivity. Hypertension and diabetes are major stressors to podocytes and pericytes, from the point of hemodynamic pressure load and cell injury. Pericytes are deeply involved in renal blood pressure regulation, through their role in controlling medullary blood flow by contraction[109]. Podocytes have mechanosensing ability and are susceptible to the change of mechanical stress, as previous studies suggest that biomechanical stress results in cytoskeletal changes in podocytes, including rearrangement of the actin cytoskeleton with loss of stress fibers and release of fatty acids from the cell membrane, subsequently activating pro-inflammatory signalling[110].

Hyperglycaemia associated with DKD has long been linked to podocyte injury, through oxidative stress, metabolic injury, foot process effacement and apoptosis. This results in nephron loss, dysregulation of α3β1 integrin, increased transforming growth factor-β1 signalling, and binding of extracellular advanced glycation-end products to

podocyte receptors[111–113]. Podocyte injury and alternation contribute to insulin resistance in type 2 diabetes. This also leads to various metabolic disturbances that interrupt endoplasmic reticulum stress response, mitochondrial signalling, actin cytoskeletal dynamics, Akt and mTOR signalling, and glucose transport, eventually causing DKD[114]. VEGF-A, a pivotal regulator of angiogenesis and vascular permeability, is indispensable for establishing and maintaining the glomerular filtration barrier due to its precise control over the proliferation and survival of recruited endothelial cells[115,116]. Podocytes is a major source of VEGF-A during fetal development and continue to secrete VEGF-A at low levels to maintain endothelial function in the mature glomerulus[117]. Hyperglycemia upregulates exuberant VEGF-A production in podocytes, leading to endothelial damage[112]. IGFBP7 has been widely reported to abolish the effects of VEGF-A, demonstrating pro-angiogenic and anti-angiogenic effects[89]. This underscores the potential critical regulatory role of IGFBP7 in podocytes.

Although a variety of cells is affected during DKD, pericytes and podocytes predominate and are sensitive to the cellular stress induced by hypertension and diabetes, providing new insights into cell-specific targeting therapy for the treatment of DKD. However, the appearance of IGFBP7 in pericytes and podocytes is the cause/consequence of DKD requires further investigation, even though clinical data already suggest that IGFBP7 elevation predicts and predate adverse renal outcomes by months to years.

4.4 IGFBP7 was elevated in cardiac vasculature before the onset of observable cardiac functional changes

Some clinical observations suggest that IGFBP7 could predict the risk of renal injury following cardiac surgery and arrest, but no study shows whether IGFBP7 could

predict the risk of cardiac dysfunction following renal complications. We noticed that the increase of IGFBP7 can occur before the observable cardiac functional changes, suggesting the possibility of using IGFBP7 to predict the risk of cardiac dysfunction. This has already been demonstrated in large clinical cohort studies[70]. However, Lin3+STZ only showed mild diastolic dysfunction in echocardiogram despite the severity of renal impairment, such as increased LVPW and IVRT, while other indicators of diastolic dysfunction such as E/A ratio and E/E' ratio, remained unchanged. Further histology and molecular studies are essential to explore more details of cardiac remodelling in our model.

It is also intriguing to notice that IGFBP7 mainly accumulated around cardiac vasculatures and was colocalized with pericytes. The interaction between pericytes and endothelial cells through soluble and membrane-bound signals effectively shields the cardiomyocytes from damage[118]. Given the position of pericytes at the interface between vessels and cardiomyocytes, they can promptly sense and be activated to pro-angiogenic state in response to cardiac stress. Activated pericytes release paracrine factors that promote tissue regeneration and revascularization[119]. Therefore, it is possible that IGFBP7 is secreted by pericytes as one of the paracrine factors during the early stage of cardiac remodelling.

4.5 Cardiorenal interaction of Lin3+STZ model

Originally, we hypothesized that Lin3+STZ could also be a cardiorenal syndrome model as the bidirectional link between the kidney and heart is often observed in patients with diabetes. However, only mild diastolic dysfunction was observed by echocardiography. According to Szymanski et al., none of the rodent models so far entirely reproduce pathophysiology and characteristics of the cardiorenal syndrome observed in

humans. The acute injury induced in one organ fails to render dysfunction in another organ, suggesting the importance of intervention in both organs during animal modeling. However, unlike human patients with chronic complications, surgery intervention or administration of exogenous substances on healthy organs may limit the clinical relevance of these animal models[120]. Compared to the traditional acute injury model, Lin3+STZ may better reflect the chronic pathogenesis of renal remodelling. Our Lin3+STZ mice showed more advanced DKD phenotypes compared to the original Lin3+STZ model from Thibodeau et al., probably due to more severe hyperglycaemia, as the original Lin3+STZ model only had a plasma glucose level of 1.733 mmol/L at the final point (18 weeks post STZ)[102]. In addition, our Lin3+STZ mice reached the endpoint at 10 weeks post-STZ, representing a consistently more accelerated DKD model. Still, more studies are needed for the development of cardiorenal mouse models to recapitulate human pathophysiology with more robust phenotypes.

5. Future Directions

5.1 Explore the Role of IGFBP7 In DKD

So far, our study revealed that IGFBP7 was significantly elevated in DKD, but whether IGFBP7 regulates renal remodelling needs further investigation. Knocking down IGFBP7 in the current disease model will allow us to understand its beneficial/detrimental role. In brief, after the last injection of STZ, mice will randomly receive a subcutaneous injection of either recombinant monoclonal anti-IGFBP7 antibody or IgG XP isotope control. Mice will be monitored up to 10 weeks post-STZ, following the same procedure. Histology analysis will be performed to see if renal phenotypes (e.g., glomerular hypertrophy and glomerulosclerosis) are improved. The preliminary data suggested that in

pressure overload HF mouse model, IGFBP7 antibody administration not only prevented the elevation of IGFBP7 in the heart, but also greatly neutralized IGFBP7 in the kidney (**Extended Data Figure 3**).

5.2 Identify if IGFBP7 specific binding to CD93 is involved in pericyte-endothelium interaction

As we have identified the localization of IGFBP7 in the kidney, namely pericytes and podocytes, we are interested in the functions and underlying mechanisms of IGFBP7 in pericytes, as well as its potential involvement in pericyte-endothelium interaction.

CD93 (also known as C1qr, C1qRp, and AA4) is a transmembrane glycoprotein belonging to the C-type lectin domain (CTLD) group 14 family[121]. Recent studies indicated that CD93 functions as one of the IGFBP7 receptors in tumor-associated endothelial cells[122], and specifically interacts with the IGF-binding domain of IGFBP7[123]. As a result, we would be interested in determining the level and localization of CD93 in diabetic kidney and heart *in vivo*. In vitro experiments will start with the culture of pericytes treated with high glucose to verify if pericytes will increase the secretion of IGFBP7 in high glucose conditions. Subsequently, the addition of exogenous IGFBP7 in siRNA-mediated CD93 knockdown (siCD93) endothelial cell line (human umbilical vein endothelial cells; HUVEC) will enable us to understand if CD93 is an important mediator in pericyte-endothelium signaling. We can also establish a pericyte and endothelial cell co-culture system to determine if the change of IGFBP7 in pericytes will affect the downstream signaling pathway in endothelial cells (PI3K/AKT and MAPK/ERK).

6. Impact & Outcome

Most of the current studies about IGFBP7 only reveal its clinical relevance as a promising cardiac and renal injury biomarker, but whether IGFBP7 plays a causal or mediator role in diabetic kidney disease is still mostly unknown. Our study, for the first time, demonstrated that IGFBP7 is significantly upregulated in DKD, specifically in the glomerular pericytes and podocytes, which is different from previous understanding obtained from AKI models. With a better understanding of the role of IGFBP7 in the glomerulus, we would be able to uncover the potential mechanisms by which IGFBP7 regulates DKD, and provide novel insights about a potential therapeutic target for diabetic kidney disease.

7. References

1. Soriano, R. M., Penfold, D. & Leslie, S. W. Anatomy, Abdomen and Pelvis: Kidneys. in *StatPearls* (StatPearls Publishing, Treasure Island (FL), 2025).
2. Sugimoto, H. *et al.* Neutralization of circulating vascular endothelial growth factor (VEGF) by anti-VEGF antibodies and soluble VEGF receptor 1 (sFlt-1) induces proteinuria. *J. Biol. Chem.* **278**, 12605–12608 (2003).
3. Munger, K. A., Kost, C. K., Brenner, B. M. & Maddox, D. A. The Renal Circulations and Glomerular Ultrafiltration. in *Brenner and Rector's The Kidney* 94–137 (Elsevier, 2012). doi:10.1016/B978-1-4160-6193-9.10003-X.
4. Scott, R. P. & Quaggin, S. E. The cell biology of renal filtration. *J. Cell Biol.* **209**, 199–210 (2015).
5. Loukopoulou, C. Renal medulla. (2024).
6. Puelles, V. G. *et al.* Glomerular number and size variability and risk for kidney disease: *Curr. Opin. Nephrol. Hypertens.* **20**, 7–15 (2011).
7. Saurus, P. Regulation of Podocyte apoptosis in Diabetic Kidney Disease - Role of SHIP2, PDK1 and CDK2. (2016).
8. Jourde-Chiche, N. *et al.* Endothelium structure and function in kidney health and disease. *Nat. Rev. Nephrol.* **15**, 87–108 (2019).
9. Schlöndorff, D. & Banas, B. The mesangial cell revisited: no cell is an island. *J. Am. Soc. Nephrol. JASN* **20**, 1179–1187 (2009).
10. American Diabetes Association. Diagnosis and Classification of Diabetes Mellitus. *Diabetes Care* **37**, S81–S90 (2014).
11. Sun, H. *et al.* IDF Diabetes Atlas: Global, regional and country-level diabetes prevalence estimates for 2021 and projections for 2045. *Diabetes Res. Clin. Pract.* **183**, 109119 (2022).
12. *Canadian Chronic Disease Surveillance System Data Files Contributed by Provinces and Territories (Data up to 2017–2018).* (2021).
13. Garg, A. X., Kiberd, B. A., Clark, W. F., Haynes, R. B. & Clase, C. M. Albuminuria and renal insufficiency prevalence guides population screening: Results from the NHANES III. *Kidney Int.* **61**, 2165–2175 (2002).

14. Liu, W., Zhou, L., Yin, W., Wang, J. & Zuo, X. Global, regional, and national burden of chronic kidney disease attributable to high sodium intake from 1990 to 2019. *Front. Nutr.* **10**, 1078371 (2023).
15. Wei, H. *et al.* Global, regional, and national burden of chronic kidney disease attributable to high fasting plasma glucose from 1990 to 2019: a systematic analysis from the global burden of disease study 2019. *Front. Endocrinol.* **15**, 1379634 (2024).
16. Ruiz-Ortega, M., Rodrigues-Diez, R. R., Lavoz, C. & Rayego-Mateos, S. Special Issue "Diabetic Nephropathy: Diagnosis, Prevention and Treatment". *J. Clin. Med.* **9**, 813 (2020).
17. Mogensen, C. E., Christensen, C. K. & Vittinghus, E. The Stages in Diabetic Renal Disease: With Emphasis on the Stage of Incipient Diabetic Nephropathy. *Diabetes* **32**, 64–78 (1983).
18. Osterby, R. Structural changes in the diabetic kidney. *Clin. Endocrinol. Metab.* **15**, 733–751 (1986).
19. Mkhize, S. Histopathological variations in diabetic nephropathy. *Int. J. Pathol. Sci.* **6**, 20–23 (2024).
20. Jain, M. Histopathological changes in diabetic kidney disease. *Clin. Queries Nephrol.* **1**, 127–133 (2012).
21. Wang, B. *et al.* E-Cadherin Expression Is Regulated by miR-192/215 by a Mechanism That Is Independent of the Profibrotic Effects of Transforming Growth Factor-β. *Diabetes* **59**, 1794–1802 (2010).
22. Derby, L., Warram, J. H., Laffel, L. M. & Krolewski, A. S. Elevated blood pressure predicts the development of persistent proteinuria in the presence of poor glycemic control, in patients with type I diabetes. *Diabete Metab.* **15**, 320–326 (1989).
23. Schmitz, A., Vaeth, M. & Mogensen, C. E. Systolic blood pressure relates to the rate of progression of albuminuria in NIDDM. *Diabetologia* **37**, 1251–1258 (1994).
24. Tanaka, Y. *et al.* Role of Glycemic Control and Blood Pressure in the Development and Progression of Nephropathy in Elderly Japanese NIDDM Patients. *Diabetes Care* **21**, 116–120 (1998).

25. Parving, H.-H. *et al.* Impaired autoregulation of glomerular filtration rate in Type 1 (insulin-dependent) diabetic patients with nephropathy. *Diabetologia* **27**, 547–552 (1984).
26. Christensen, P. K., Hansen, H. P. & Parving, H.-H. Impaired autoregulation of GFR in hypertensive non-insulin dependent diabetic patients. *Kidney Int.* **52**, 1369–1374 (1997).
27. UK Prospective Diabetes Study Group. Tight blood pressure control and risk of macrovascular and microvascular complications in type 2 diabetes: UKPDS 38. UK Prospective Diabetes Study Group. *BMJ* **317**, 703–713 (1998).
28. Strippoli, G. F. M., Craig, M., Deeks, J. J., Schena, F. P. & Craig, J. C. Effects of angiotensin converting enzyme inhibitors and angiotensin II receptor antagonists on mortality and renal outcomes in diabetic nephropathy: systematic review. *BMJ* **329**, 828 (2004).
29. Lewis, E. J., Hunsicker, L. G., Bain, R. P. & Rohde, R. D. The Effect of Angiotensin-Converting-Enzyme Inhibition on Diabetic Nephropathy. *N. Engl. J. Med.* **329**, 1456–1462 (1993).
30. Atkins, R. C. *et al.* Proteinuria reduction and progression to renal failure in patients with type 2 diabetes mellitus and overt nephropathy. *Am. J. Kidney Dis. Off. J. Natl. Kidney Found.* **45**, 281–287 (2005).
31. Smith, D. K., Lennon, R. P. & Carlsgaard, P. B. Managing Hypertension Using Combination Therapy. *Am. Fam. Physician* **101**, 341–349 (2020).
32. Tobe, S. W. *et al.* Cardiovascular and Renal Outcomes With Telmisartan, Ramipril, or Both in People at High Renal Risk: Results From the ONTARGET and TRANSCEND Studies. *Circulation* **123**, 1098–1107 (2011).
33. Agarwal, R. *et al.* Cardiovascular and kidney outcomes with finerenone in patients with type 2 diabetes and chronic kidney disease: the FIDELITY pooled analysis. *Eur. Heart J.* **43**, 474–484 (2022).
34. Chalmers, J. & Cooper, M. E. UKPDS and the Legacy Effect. *N. Engl. J. Med.* **359**, 1618–1620 (2008).

35. De Boer, I. H. & for the DCCT/EDIC Research Group. Kidney Disease and Related Findings in the Diabetes Control and Complications Trial/Epidemiology of Diabetes Interventions and Complications Study. *Diabetes Care* **37**, 24–30 (2014).
36. Holman, R. R., Paul, S. K., Bethel, M. A., Matthews, D. R. & Neil, H. A. W. 10-Year Follow-up of Intensive Glucose Control in Type 2 Diabetes. *N. Engl. J. Med.* **359**, 1577–1589 (2008).
37. Intensive Blood Glucose Control and Vascular Outcomes in Patients with Type 2 Diabetes. *N. Engl. J. Med.* **358**, 2560–2572 (2008).
38. Baigent, C. *et al.* Impact of diabetes on the effects of sodium glucose co-transporter-2 inhibitors on kidney outcomes: collaborative meta-analysis of large placebo-controlled trials. *The Lancet* **400**, 1788–1801 (2022).
39. Mann, J. F. E. *et al.* Liraglutide and Renal Outcomes in Type 2 Diabetes. *N. Engl. J. Med.* **377**, 839–848 (2017).
40. Yaribeygi, H., Atkin, S. L., Montecucco, F., Jamialahmadi, T. & Sahebkar, A. Renoprotective Effects of Incretin-Based Therapy in Diabetes Mellitus. *BioMed Res. Int.* **2021**, 8163153 (2021).
41. Nauck, M. A., Quast, D. R., Wefers, J. & Meier, J. J. GLP-1 receptor agonists in the treatment of type 2 diabetes - state-of-the-art. *Mol. Metab.* **46**, 101102 (2021).
42. FinnDiane Study Group *et al.* Lipid abnormalities predict progression of renal disease in patients with type 1 diabetes. *Diabetologia* **52**, 2522–2530 (2009).
43. Thomas, M. C. *et al.* Serum Lipids and the Progression of Nephropathy in Type 1 Diabetes. *Diabetes Care* **29**, 317–322 (2006).
44. Haynes, R. *et al.* Effects of lowering LDL cholesterol on progression of kidney disease. *J. Am. Soc. Nephrol. JASN* **25**, 1825–1833 (2014).
45. The Emerging Risk Factors Collaboration. Diabetes mellitus, fasting blood glucose concentration, and risk of vascular disease: a collaborative meta-analysis of 102 prospective studies. *The Lancet* **375**, 2215–2222 (2010).
46. Fried, L. F. *et al.* Renal insufficiency as a predictor of cardiovascular outcomes and mortality in elderly individuals. *J. Am. Coll. Cardiol.* **41**, 1364–1372 (2003).
47. George, L. K. *et al.* Heart Failure Increases the Risk of Adverse Renal Outcomes in Patients With Normal Kidney Function. *Circ. Heart Fail.* **10**, e003825 (2017).

48. Thomas, M. C. *et al.* Diabetic kidney disease. *Nat. Rev. Dis. Primer* **1**, 15018 (2015).
49. Clemmons, D. R. 40 YEARS OF IGF1: Role of IGF-binding proteins in regulating IGF responses to changes in metabolism. *J. Mol. Endocrinol.* **61**, T139–T169 (2018).
50. Baxter, R. C. Signaling Pathways of the Insulin-like Growth Factor Binding Proteins. *Endocr. Rev.* **44**, 753–778 (2023).
51. Galal, M. A. *et al.* Insulin Receptor Isoforms and Insulin Growth Factor-like Receptors: Implications in Cell Signaling, Carcinogenesis, and Chemoresistance. *Int. J. Mol. Sci.* **24**, 15006 (2023).
52. Werner, H. The IGF1 Signaling Pathway: From Basic Concepts to Therapeutic Opportunities. *Int. J. Mol. Sci.* **24**, 14882 (2023).
53. Vorwerk, P., Hohmann, B., Oh, Y., Rosenfeld, R. G. & Shymko, R. M. Binding Properties of Insulin-Like Growth Factor Binding Protein-3 (IGFBP-3), IGFBP-3 N- and C-Terminal Fragments, and Structurally Related Proteins mac25 and Connective Tissue Growth Factor Measured Using a Biosensor. *Endocrinology* **143**, 1677–1685 (2002).
54. Zhou, H. *et al.* Regulatory mechanisms and therapeutic implications of insulin-like growth factor 2 mRNA-binding proteins, the emerging crucial m^6 A regulators of tumors. *Theranostics* **13**, 4247–4265 (2023).
55. Fowlkes, J. L., Thrailkill, K. M., George-Nascimento, C., Rosenberg, C. K. & Serra, D. M. Heparin-Binding, Highly Basic Regions within the Thyroglobulin Type-1 Repeat of Insulin-Like Growth Factor (IGF)-Binding Proteins (IGFBPs) -3, -5, and -6 Inhibit IGFBP-4 Degradation*. *Endocrinology* **138**, 2280–2285 (1997).
56. Akaogi, K. *et al.* Cell Adhesion Activity of a 30-kDa Major Secreted Protein from Human Bladder Carcinoma Cells. *Biochem. Biophys. Res. Commun.* **198**, 1046–1053 (1994).
57. The Human Protein Atlas. Tissue expression of IGFBP7.
58. Yamanaka, Y., Wilson, E. M., Rosenfeld, R. G. & Oh, Y. Inhibition of Insulin Receptor Activation by Insulin-like Growth Factor Binding Proteins. *J. Biol. Chem.* **272**, 30729–30734 (1997).

59. Liu, Y. *et al.* Serum IGFBP7 levels associate with insulin resistance and the risk of metabolic syndrome in a Chinese population. *Sci. Rep.* **5**, 10227 (2015).
60. Ma, Y. *et al.* Tumor suppressor gene insulin-like growth factor binding protein-related protein 1 (IGFBP-rP1) induces senescence-like growth arrest in colorectal cancer cells. *Exp. Mol. Pathol.* **85**, 141–145 (2008).
61. Ruan, W. *et al.* IGFBP7 plays a potential tumor suppressor role in colorectal carcinogenesis. *Cancer Biol. Ther.* **6**, 354–359 (2007).
62. Ruan, W. *et al.* IGFBP7 plays a potential tumor suppressor role against colorectal carcinogenesis with its expression associated with DNA hypomethylation of exon 1. *J. Zhejiang Univ. Sci. B* **7**, 929–932 (2006).
63. Vizioli, M. G. *et al.* IGFBP7: an oncosuppressor gene in thyroid carcinogenesis. *Oncogene* **29**, 3835–3844 (2010).
64. Gandhi, P. U. *et al.* Prognostic Usefulness of Insulin-Like Growth Factor-Binding Protein 7 in Heart Failure With Reduced Ejection Fraction: A Novel Biomarker of Myocardial Diastolic Function? *Am. J. Cardiol.* **114**, 1543–1549 (2014).
65. Adamson, C. *et al.* IGFBP-7 and Outcomes in Heart Failure With Reduced Ejection Fraction. *JACC Heart Fail.* **11**, 291–304 (2023).
66. Barroso, M. C. *et al.* Serum insulin-like growth factor-1 and its binding protein-7: potential novel biomarkers for heart failure with preserved ejection fraction. *BMC Cardiovasc. Disord.* **16**, 199 (2016).
67. Gandhi, P. U. *et al.* Insulin-Like Growth Factor–Binding Protein-7 as a Biomarker of Diastolic Dysfunction and Functional Capacity in Heart Failure With Preserved Ejection Fraction. *JACC Heart Fail.* **4**, 860–869 (2016).
68. Januzzi, J. L. *et al.* IGFBP7 (Insulin-Like Growth Factor–Binding Protein-7) and Neprilysin Inhibition in Patients With Heart Failure. *Circ. Heart Fail.* **11**, e005133 (2018).
69. Bracun, V. *et al.* Insulin-like growth factor binding protein 7 (IGFBP7), a link between heart failure and senescence. *ESC Heart Fail.* **9**, 4167–4176 (2022).
70. Abou Kamar, S. *et al.* Association of baseline and longitudinal changes in insulin-like growth factor-binding protein-7 with the risk of incident heart failure: Data

from the PREVEND study. *Eur. J. Heart Fail.* ejhf.3328 (2024) doi:10.1002/ejhf.3328.

71. Ahmed, A. *et al.* Elevated plasma sRAGE and IGFBP7 in heart failure decrease after heart transplantation in association with haemodynamics. *ESC Heart Fail.* **7**, 2340–2353 (2020).
72. Hage, C. *et al.* Comparison of Prognostic Usefulness of Serum Insulin-Like Growth Factor-Binding Protein 7 in Patients With Heart Failure and Preserved Versus Reduced Left Ventricular Ejection Fraction. *Am. J. Cardiol.* **121**, 1558–1566 (2018).
73. Lisowska, A. *et al.* Insulin-like growth factor-binding protein 7 (IGFBP 7) as a new biomarker in coronary heart disease. *Adv. Med. Sci.* **64**, 195–201 (2019).
74. Lisowska, A. *et al.* IGFBP7 Concentration May Reflect Subclinical Myocardial Damage and Kidney Function in Patients with Stable Ischemic Heart Disease. *Biomolecules* **12**, 274 (2022).
75. Ibrahim, N. E. *et al.* Diagnostic and Prognostic Utilities of Insulin-Like Growth Factor Binding Protein-7 in Patients With Dyspnea. *JACC Heart Fail.* **8**, 415–422 (2020).
76. Ferreira, J. P. *et al.* Insulin-like growth factor binding protein-7 concentrations in chronic heart failure: Results from the EMPEROR programme. *Eur. J. Heart Fail.* **26**, 806–816 (2024).
77. Kashani, K. *et al.* Discovery and validation of cell cycle arrest biomarkers in human acute kidney injury. *Crit. Care* **17**, R25 (2013).
78. Bihorac, A. *et al.* Validation of Cell-Cycle Arrest Biomarkers for Acute Kidney Injury Using Clinical Adjudication. *Am. J. Respir. Crit. Care Med.* **189**, 932–939 (2014).
79. Ferrari, F. *et al.* Routine Adoption of Urinary [IGFBP7]·[TIMP-2] to Assess Acute Kidney Injury at Any Stage 12 hours After Intensive Care Unit Admission: a Prospective Cohort Study. *Sci. Rep.* **9**, 16484 (2019).
80. US Food and Drug Administration. (2014).
81. Guzzi, L. M. *et al.* Clinical use of [TIMP-2]•[IGFBP7] biomarker testing to assess risk of acute kidney injury in critical care: guidance from an expert panel. *Crit. Care* **23**, 225 (2019).

82. Meersch, M. *et al.* Urinary TIMP-2 and IGFBP7 as Early Biomarkers of Acute Kidney Injury and Renal Recovery following Cardiac Surgery. *PLoS ONE* **9**, e93460 (2014).
83. Pilarczyk, K. *et al.* Urinary [TIMP-2]*[IGFBP7] for early prediction of acute kidney injury after coronary artery bypass surgery. *Ann. Intensive Care* **5**, 50 (2015).
84. Adler, C. *et al.* TIMP-2/IGFBP7 predicts acute kidney injury in out-of-hospital cardiac arrest survivors. *Crit. Care* **22**, 126 (2018).
85. Titeca-Beauport, D. *et al.* The urine biomarkers TIMP2 and IGFBP7 can identify patients who will experience severe acute kidney injury following a cardiac arrest: A prospective multicentre study. *Resuscitation* **141**, 104–110 (2019).
86. MacMillan, Y. S., Mamas, M. A. & Sun, L. Y. IGFBP7 as a preoperative predictor of congestive acute kidney injury after cardiac surgery. *Open Heart* **9**, e002027 (2022).
87. Huang, F. *et al.* Predictive value of urinary cell cycle arrest biomarkers for all cause-acute kidney injury: a meta-analysis. *Sci. Rep.* **13**, 6037 (2023).
88. Januzzi, J. L. *et al.* Insulin-Like Growth Factor Binding Protein 7 Predicts Renal and Cardiovascular Outcomes in the Canagliflozin Cardiovascular Assessment Study. *Diabetes Care* **44**, 210–216 (2021).
89. Lit, K. K., Zhirenova, Z. & Blocki, A. Insulin-like growth factor-binding protein 7 (IGFBP7): A microenvironment-dependent regulator of angiogenesis and vascular remodeling. *Front. Cell Dev. Biol.* **12**, 1421438 (2024).
90. Zhang, L. *et al.* Insulin-like growth factor-binding protein-7 (IGFBP7) links senescence to heart failure. *Nat. Cardiovasc. Res.* **1**, 1195–1214 (2022).
91. Ko, T. *et al.* Cardiac fibroblasts regulate the development of heart failure via Htra3-TGF-β-IGFBP7 axis. *Nat. Commun.* **13**, 3275 (2022).
92. Katoh, M. *et al.* Vaccine Therapy for Heart Failure Targeting the Inflammatory Cytokine Igfbp7. *Circulation* **150**, 374–389 (2024).
93. Yu, J. *et al.* Insulin-like growth factor binding protein 7 promotes acute kidney injury by alleviating poly ADP ribose polymerase 1 degradation. *Kidney Int.* **102**, 828–844 (2022).
94. Yu, J. *et al.* Renal tubular epithelial IGFBP7 interacts with PKM2 to drive renal lipid accumulation and fibrosis. *Mol. Ther.* **33**, 3757–3777 (2025).

95. Watanabe, J. *et al.* Role of IGFBP7 in Diabetic Nephropathy: TGF-β1 Induces IGFBP7 via Smad2/4 in Human Renal Proximal Tubular Epithelial Cells. *PLOS ONE* **11**, e0150897 (2016).
96. Emlet, D. R. *et al.* Insulin-like growth factor binding protein 7 and tissue inhibitor of metalloproteinases-2: differential expression and secretion in human kidney tubule cells. *Am. J. Physiol.-Ren. Physiol.* **312**, F284–F296 (2017).
97. Schanz, M., Kimmel, M., Alscher, M. D., Amann, K. & Daniel, C. TIMP-2 and IGFBP7 in human kidney biopsies in renal disease. *Clin. Kidney J.* **16**, 1434–1446 (2023).
98. Azushima, K., Gurley, S. B. & Coffman, T. M. Modelling diabetic nephropathy in mice. *Nat. Rev. Nephrol.* **14**, 48–56 (2018).
99. Brosius, F. C. *et al.* Mouse Models of Diabetic Nephropathy. *J. Am. Soc. Nephrol.* **20**, 2503–2512 (2009).
100. Furman, B. L. Streptozotocin-Induced Diabetic Models in Mice and Rats. *Curr. Protoc.* **1**, e78 (2021).
101. Touyz, R. M. *et al.* Angiotensin II-Dependent Chronic Hypertension and Cardiac Hypertrophy Are Unaffected by gp91phox-Containing NADPH Oxidase. *Hypertension* **45**, 530–537 (2005).
102. Thibodeau, J.-F. *et al.* A Novel Mouse Model of Advanced Diabetic Kidney Disease. *PLoS ONE* **9**, e113459 (2014).
103. Zhao, H. J. *et al.* Endothelial Nitric Oxide Synthase Deficiency Produces Accelerated Nephropathy in Diabetic Mice. *J. Am. Soc. Nephrol.* **17**, 2664–2669 (2006).
104. Yuen, D. A. *et al.* Culture-Modified Bone Marrow Cells Attenuate Cardiac and Renal Injury in a Chronic Kidney Disease Rat Model via a Novel Antifibrotic Mechanism. *PLoS ONE* **5**, e9543 (2010).
105. Boorsma, E. M. *et al.* Congestion in heart failure: a contemporary look at physiology, diagnosis and treatment. *Nat. Rev. Cardiol.* **17**, 641–655 (2020).
106. Januzzi, J. L. *et al.* Cardiorenal Biomarkers, Canagliflozin, and Outcomes in Diabetic Kidney Disease: The CREDENCE Trial. *Circulation* **148**, 651–660 (2023).

107. Helal, I., Fick-Brosnahan, G. M., Reed-Gitomer, B. & Schrier, R. W. Glomerular hyperfiltration: definitions, mechanisms and clinical implications. *Nat. Rev. Nephrol.* **8**, 293–300 (2012).
108. Bramlage, P. *et al.* Renal function deterioration in adult patients with type-2 diabetes. *BMC Nephrol.* **21**, 312 (2020).
109. Shaw, I., Rider, S., Mullins, J., Hughes, J. & Péault, B. Pericytes in the renal vasculature: roles in health and disease. *Nat. Rev. Nephrol.* **14**, 521–534 (2018).
110. Sharma, M. *et al.* Glomerular Biomechanical Stress and Lipid Mediators during Cellular Changes Leading to Chronic Kidney Disease. *Biomedicines* **10**, 407 (2022).
111. Sawada, K. *et al.* Upregulation of α 3 β 1-Integrin in Podocytes in Early-Stage Diabetic Nephropathy. *J. Diabetes Res.* **2016**, 1–7 (2016).
112. Iglesias-de La Cruz, M. C. *et al.* Effects of high glucose and TGF-β1 on the expression of collagen IV and vascular endothelial growth factor in mouse podocytes. *Kidney Int.* **62**, 901–913 (2002).
113. Rabbani, N. & Thornalley, P. J. Advanced glycation end products in the pathogenesis of chronic kidney disease. *Kidney Int.* **93**, 803–813 (2018).
114. Lay, A. C. & Coward, R. J. M. The Evolving Importance of Insulin Signaling in Podocyte Health and Disease. *Front. Endocrinol.* **9**, 693 (2018).
115. Eremina, V. *et al.* Glomerular-specific alterations of VEGF-A expression lead to distinct congenital and acquired renal diseases. *J. Clin. Invest.* **111**, 707–716 (2003).
116. Eremina, V., Baelde, H. J. & Quaggin, S. E. Role of the VEGF-A Signaling Pathway in the Glomerulus: Evidence for Crosstalk between Components of the Glomerular Filtration Barrier. *Nephron Physiol.* **106**, p32–p37 (2007).
117. Hu, S. *et al.* Crosstalk among podocytes, glomerular endothelial cells and mesangial cells in diabetic kidney disease: an updated review. *Cell Commun. Signal.* **22**, 136 (2024).
118. Avolio, E., Campagnolo, P., Katare, R. & Madeddu, P. The role of cardiac pericytes in health and disease: therapeutic targets for myocardial infarction. *Nat. Rev. Cardiol.* **21**, 106–118 (2024).

119. Mayo, J. N. & Bearden, S. E. Driving the Hypoxia-Inducible Pathway in Human Pericytes Promotes Vascular Density in an Exosome-Dependent Manner. *Microcirculation* **22**, 711–723 (2015).
120. Szymanski, M. K., De Boer, R. A., Navis, G. J., Van Gilst, W. H. & Hillege, H. L. Animal models of cardiorenal syndrome: a review. *Heart Fail. Rev.* **17**, 411–420 (2012).
121. Li, Y. *et al.* Angiogenesis modulated by CD93 and its natural ligands IGFBP7 and MMRN2: a new target to facilitate solid tumor therapy by vasculature normalization. *Cancer Cell Int.* **23**, 189 (2023).
122. Sun, Y. *et al.* Blockade of the CD93 pathway normalizes tumor vasculature to facilitate drug delivery and immunotherapy. *Sci. Transl. Med.* **13**, eabc8922 (2021).
123. Xu, Y., Sun, Y., Zhu, Y. & Song, G. Structural insight into CD93 recognition by IGFBP7. *Structure* **32**, 282-291.e4 (2024).

8. Extended Data

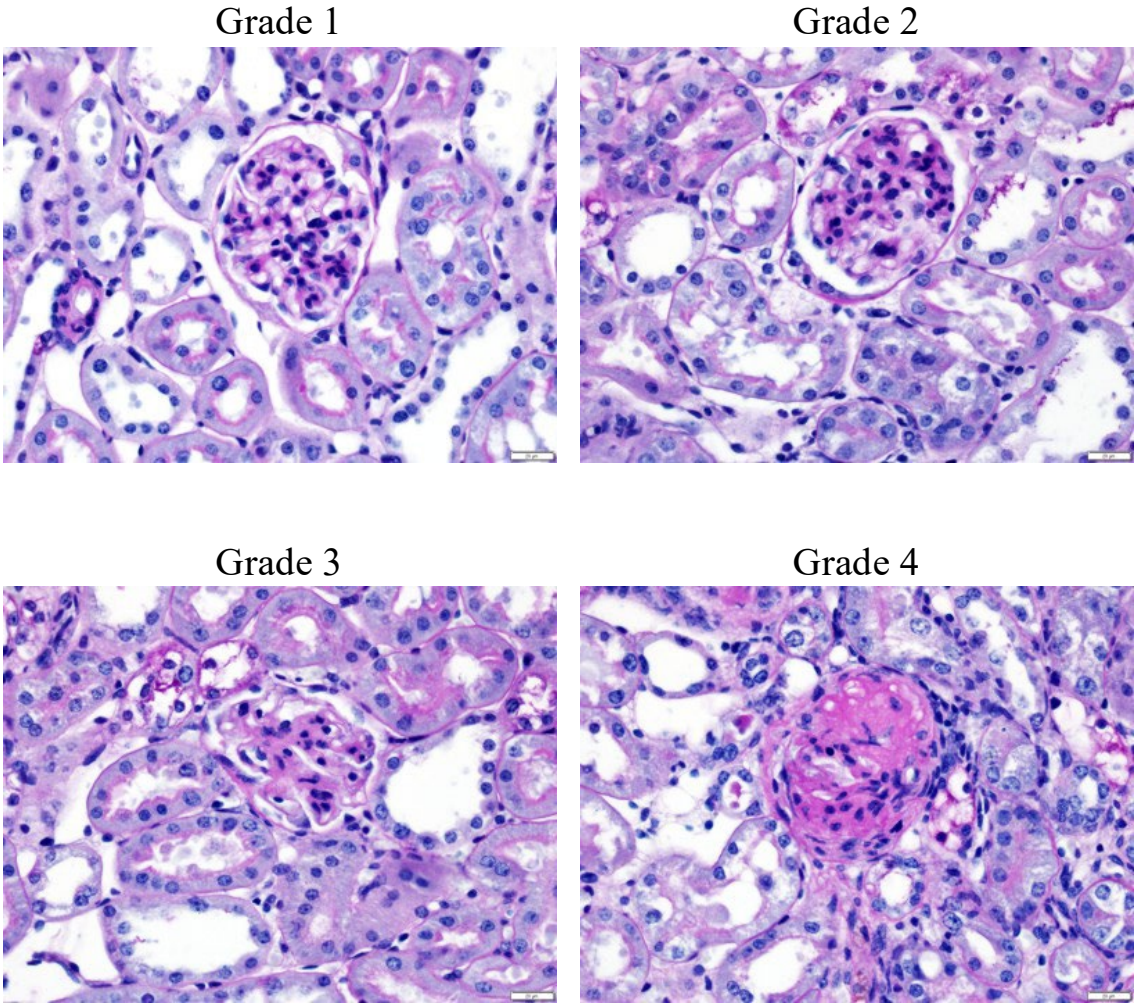

Extended Data Figure 1 Representative images of semi-quantitative analysis of glomerulosclerosis. Grade 1, normal or sclerotic area up to 25% (minimal); Grade 2, sclerotic area 25-50% (moderate); Grade 3, sclerotic area 50-75% (moderate to severe), and Grade 4, sclerotic area 75-100% (severe). Grading criteria include mesangial expansion and capillary occlusion. Scale bar=20 μm.

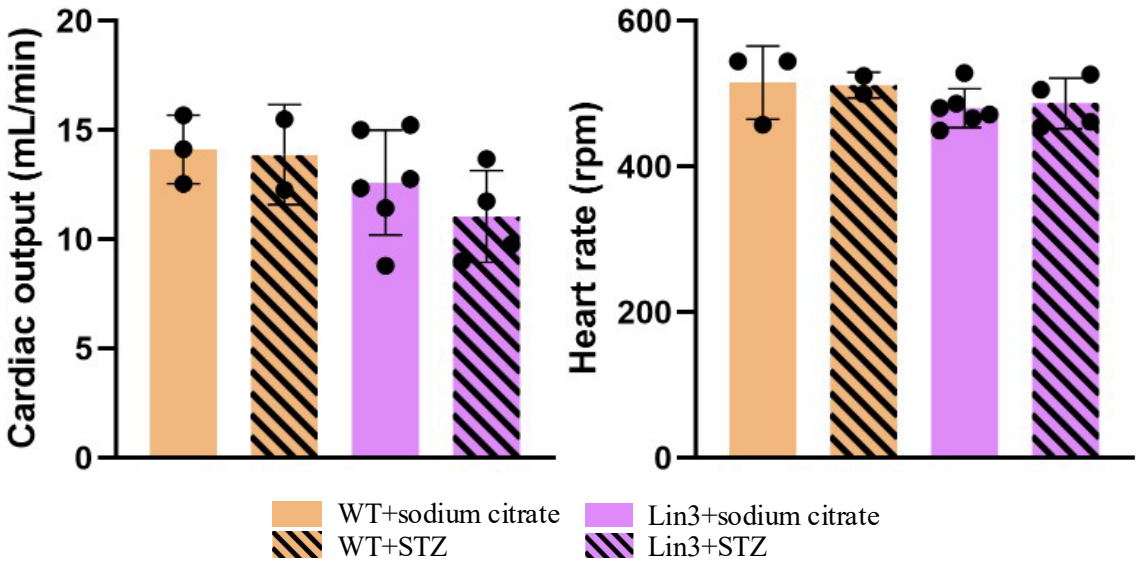

Extended Data Figure 2 No significant differences in cardiac output and heart rate in males at 10 weeks post STZ. (A) No significant difference in cardiac output was observed in different male groups. (B) No significant difference in heart rate was observed in different male groups, but Lin3+STZ males showed slightly decreased heart rate compared to WT+sodium citrate (mean heart rate 486 rpm vs. 515 rpm). n=2-6 per group. All values are presented as mean ± s.d. $P<0.05$ was considered statistically significant. P values were calculated using one-way ANOVA with Tukey's correction.

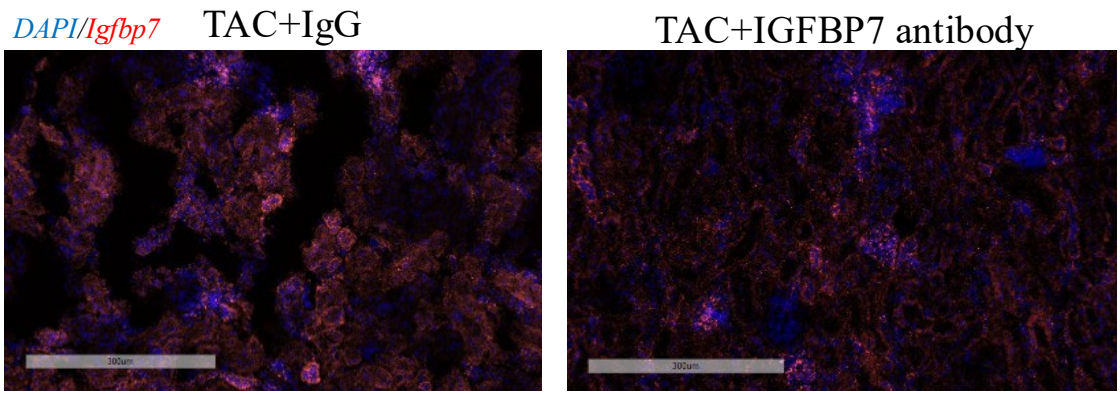

Extended Data Figure 3 Igfbp7 was neutralized in the kidney with subcutaneous injection of IGFBP7 antibody. Transcriptional level of Igfbp7 was determined by RNA in situ hybridization in the pressure overload HF mouse model. IGFBP7 antibody greatly reduced the elevation of Igfbp7 in the kidney (right) compared to IgG control (left). Scale bar=300 μm.